EUROPEAN CENTRAL BANK
EUROSYSTEM

Working Paper Series

Sarah Spiteri, Léonore Lebouteiller,
Nicole Vorderobermeier, Mar Delgado-Téllez,
Andrej Ceglar

Beat the heat, the role of heat waves and droughts in regional EU economies

No 3248

Abstract

Europe is increasingly exposed to heat waves and droughts, but their short-term economic effects across sectors remain hard to predict. This study develops climate-augmented models to predict real growth in per capita value added across 1,117 EU regions (2002–2022), by combining economic indicators with high-frequency climate data. When using machine learning (ML, Random Forest and XGBoost), climate variables improve predictions in agriculture, while gains for other sectors are limited and do not outperform economic models. Heat wave indicators consistently enhance predictive performance, whereas drought effects vary by sector. Simulations of extreme combined heat and drought scenarios suggest that agricultural annual growth could fall by 1.9 to 7.6 percentage points in most regions, whereas industry, and manufacturing in particular, is less affected, although impacts are more pronounced in eastern Europe and the Baltic states. Overall, ML models better reflect complex climate–economic interactions, supporting their use for early warning, policy planning, and targeted adaptation.

Keywords: climate extremes, regional predictions, machine learning, production.

JEL Classification: C53, E37, Q54, R15.

Non-Technical Summary

Extreme climate events, particularly heat waves and droughts, are becoming more frequent, longer lasting, and more spatially widespread in Europe. These developments raise important questions for policymakers about how such events affect regional economic activity in the short-run and how these effects differ between sectors and locations. This paper contributes to this discussion by developing climate-augmented predictive models for regional gross value added (GVA) per capita growth at the NUTS-3 level, covering 1,117 European Union (EU) regions during the period 2002–2022, for the agricultural sector, the industrial sector (an aggregate encompassing mining, manufacturing, energy, and water supply) and manufacturing as a stand-alone sector.

The analysis combines annual economic variables with high-frequency climate indicators from the Copernicus European Drought Observatory. These indicators capture different dimensions of climate stress: heat waves, meteorological droughts (precipitation deficits), hydrological droughts (low river flows), and agricultural droughts (soil moisture and vegetation stress). We also construct measures of compounding events, periods in which heat waves and droughts occur simultaneously, and indicators capturing climate conditions in neighbouring regions, reflecting the spatial propagation of climate shocks.

We combine three approaches: annual aggregation, principal component analysis, and mixed data sampling. The predictive performance of ML models (Random Forest and XGBoost) is assessed using an out-of-sample rolling window for the period 2018-2022 against a linear benchmark. In addition, climate-augmented models are assessed relative to the performance of models using only economic data and regional controls.

The results suggest that both of our ML models substantially improved the predictive accuracy of climate-augmented models relative to linear specifications, particularly in climate-sensitive sectors. The most pronounced gains arise in agriculture, where the heat wave and drought indicators provide meaningful predictive power. The industrial aggregate shows modest improvements in predictive accuracy, primarily reflecting the ability of ML models to capture complex nonlinear patterns rather than the contribution of climate-related variables. In contrast, the stand-alone manufacturing performance appears largely unchanged by the inclusion of climatological information. In addition, climate information enhances predictive performance only in nonlinear models. Linear climate-augmented specifications do not outperform economic-only benchmarks, suggesting that the economic effects of climate extremes operate through nonlinear channels that linear predictive

models cannot represent.

The paper employs the XGBoost model with among the lowest RMSEs in the predictive exercise to simulate the economic effects of an extreme compound heat wave and drought scenario, similar to the conditions observed in 2022. The results indicate substantial losses in real GVA per capita growth in the agricultural sector, averaging −4.54 percentage points (pp) relative to a no-anomaly benchmark, with the most pronounced impacts concentrated in eastern Europe. By contrast, industrial sectors experience smaller but still meaningful reductions (on average −0.75 pp), while manufacturing remains broadly stable (on average −0.11 pp), particularly in eastern Europe and the Baltic countries.

These heterogeneous effects likely reflect differences in exposure, adaptive capacity, irrigation infrastructure, and the degree of reliance on indoor production environments. In particular, the greater vulnerability of agriculture is consistent with limited adaptive capacity and the predominance of rain-fed systems in affected regions, whereas the relative resilience of manufacturing may stem from the buffering role of indoor production conditions against extreme heat and drought. These results present aggregated outcomes, which obscure yearly heterogeneities between 2002 and 2022.

In general, the findings highlight the importance of integrating climate information into short-term economic monitoring tools. Climate-augmented predictions using ML methods can support the identification of sectors and regions most exposed to compounding climate extremes, to support policymaking and guide the design of targeted and effective adaptation strategies.

1 Introduction

Europe is entering a period of increasing and concurrent climate risks, where extreme events such as droughts and heat waves increasingly interact and cascade across sectors, amplifying socio-economic impacts (European Environment Agency, 2024). During the past decade, large parts of the continent have experienced historically exceptional severe drought conditions (Toreti et al., 2019, 2024). Repeated winters with below-average precipitation, reduced mountain snowpack, and summer rainfall deficits have reduced river discharge, lowered water reservoirs, and limited hydroelectric and thermal power production. Agriculture has been particularly affected, with reduced soil moisture causing widespread vegetation stress and decreased crop yields in the European Union (EU). The 2022 drought illustrates the intensity of these extremes. Hot and dry conditions drove significant yield losses (Pinke et al., 2024; Baruth et al., 2022), critically depleted water availability in regions such as the Po River Basin, induced saltwater intrusion in delta areas, and forced water-use restrictions in southern and western Europe. These shortages also triggered disruptions beyond agriculture, including impacts on ecosystems (European Environment Agency, 2025), curtailed inland shipping on the Rhine, reduced hydropower generation, shutdowns of alpine hydroelectric facilities, and heightened wildfire activity in southwestern Europe (Bevacqua et al., 2024; Toreti et al., 2022).

Despite their increasing frequency, the economic impacts of droughts and heat waves remain insufficiently quantified, especially for advanced economies. Evidence shows that extreme droughts can depress the growth of gross domestic product (GDP) for several years, with regional output in Europe remaining up to three percentage points (pp) lower four years after a major drought event (Usman et al., 2025a). Moreover, droughts and harvest failures have substantial inflationary effects: harvest shocks explain roughly 30% of medium-term volatility in euro area inflation (Peersman, 2022), and single crop shocks can raise food prices by double digits with persistent inflationary consequences (Wegner et al., 2025; Parker, 2016; Beirne et al., 2021; Kotz et al., 2025). Beyond agriculture, drought-driven disruptions to river transport, electricity generation, water-dependent manufacturing, and tourism further propagate through production networks and supply chains, increasing costs, and constraining output. These dynamics can also affect financial institutions through higher credit risk, reduced collateral values, operational disruptions, and market volatility.

A growing body of evidence highlights the importance of compounding hazards, such as simultaneous droughts and heat waves, droughts combined with reduced surface or groundwater availability, or heat waves coupled with the risk of wildfires, in shaping the overall impact on firms, sectors,

and financial institutions. For example, the German power sector has been shown to be highly vulnerable to droughts and heat waves, which often co-occur and jointly exacerbate challenges such as power plant outages and electricity price volatility (Golub et al., 2022). Healthy ecosystems can buffer some of these effects, while degraded ecosystems can amplify them. Nature-related risks, particularly water scarcity, are increasingly recognised as dominant transmission channels for the economy of the euro area and its banking sector (Ceglar et al., 2025). More than 40% of bank lending is concentrated in firms highly exposed to drought and strongly dependent on surface water provision, with exposures especially pronounced in southern and western Europe. However, empirical evidence on the compound effects of heat waves and droughts on non-agricultural sectors, particularly manufacturing, remains limited. This gap prevents a full understanding of how these shocks propagate through value chains and how they can generate systemic financial risks.

Research that quantifies the macroeconomic consequences of climate extremes relies predominantly on linear econometric and structural macroeconomic frameworks. Usman et al. (2025a) employ panel regression techniques to estimate persistent GDP losses following major drought events, identifying regional output reductions lasting up to four years after the shock. Peersman (2022) uses a structural vector autoregression model to attribute medium-term inflation volatility in the euro area to harvest disruptions, while Wegner et al. (2025); Parker (2016); Beirne et al. (2021); Kotz et al. (2025) adopt semi-structural and reduced-form approaches to trace the transmission of crop failures into food prices and broader inflationary dynamics. These methodologies typically draw on historical time-series data and leverage exogenous climate shocks as instruments or controls to isolate causal effects. Although well-suited for aggregate analysis, they often abstract from sectoral heterogeneity and nonlinear interactions, limiting their capacity to capture compounding risks and spatially granular impacts.

The integration of climate and economic data through machine learning (ML) for macroeconomic predictions remains relatively unexplored. A notable contribution is Rossi et al. (2023), who applied an ML-based framework to quantify drought-related risks across interconnected European systems, including agriculture, water supply, energy, river transport, and terrestrial and freshwater ecosystems, estimating sector- and region-specific economic losses under both present and projected climate conditions. Their methodology involved constructing a harmonised impact dataset by combining historical climate observations (1979–2021) with sectoral vulnerability indicators derived from economic and biophysical data. To isolate climate-driven variability, the data were detrended and aggregated into discrete vulnerability classes. Decision Tree Classifiers were then trained on

these classes to predict drought-induced losses. The trained models were subsequently used for scenario-based simulations under multiple greenhouse gas concentration pathways, enabling probabilistic assessments of future drought risks and cascading economic impacts.

Building on this foundation, we adopt a predictive framework using a similar set of climate indicators to Usman et al. (2025a,b) to model the predictive role of heat waves and droughts with two ensemble tree-based algorithms, Random Forest and XGBoost, to improve predictive accuracy and generalisation. We apply climate-augmented models for regional real sectoral gross value added (GVA) per capita growth, focussing on climate-exposed sectoral NACE aggregations: agriculture (sector A), industry excluding construction (sector B-E),[1] and, also modelled separately, manufacturing (sector C). These sectors have been identified as potential targets for climate policies (Battiston et al., 2022). This approach shifts the focus of analysis from inferential effects to predicted outcomes. Predictive performance is evaluated across sectors and compared with a linear benchmark. Our approach uses a rich dataset encompassing cross-country, within-country, and cross-sectoral variation. This heterogeneity enables a rigorous evaluation of how economic activity responds to climate conditions in linear and nonlinear predictive models. We also assess the compound predicted consequences of overlapping climate events and regional spillovers. We reconcile annual economic indicators with daily climate observations using aggregation (annual medians and variability) and feature-extraction techniques such as principal component analysis (PCA) and mixed data sampling (MIDAS) to capture nonlinear and lagged climate effects.

The results of the predictive exercise indicate that climate-augmented ML models significantly outperform linear counterparts in agriculture, which is sensitive to climate extremes, where heat wave and drought indicators drive predictive gains. The industrial aggregate (sectors B-E) exhibits modest gains in predictive accuracy, largely attributable to the capacity of ML models to capture complex nonlinear relationships rather than to the inclusion of climate-related variables. By contrast, predictive performance in the manufacturing sector remains broadly unaffected by the incorporation of climatological information. Climate-augmented linear models offer no statistically significant improvement over economic baselines, whereas ensemble ML methods capture complex interactions and sectoral heterogeneity. Among climate specifications, simple aggregation of climate variables often matches or exceeds PCA and MIDAS in predictive accuracy, underscoring its robustness in short panels. An analysis of feature importance reveals that economic variables

[1] Sector B-E encompasses mining and quarrying (B), manufacturing (C), electricity, gas, steam, and air conditioning supply (D), as well as water supply, sewerage, waste management, and remediation activities (E).

dominate predictions, but climate indicators, especially heat waves, provide meaningful contributions, with effects varying by sector, region, and season. These findings highlight the importance of nonlinear models and mixed-frequency approaches for real-time climate–economic predictions.

To complement our predictive analysis, we use the XGBoost model that achieved amongst the lowest RMSEs in our predictive exercise to quantify the incremental effect of compound extremes similar to the climate conditions that occurred in 2022 on GVA per capita growth by sector averaged over the years 2002 to 2022. Relative to a no-anomaly climate benchmark, the compound scenario yields the largest simulated losses in agriculture, with average losses of 4.54 pp, with the most severe impacts concentrated in eastern Europe. By contrast, southern Europe exhibits more muted impacts, in tension with Cammalleri et al. (2020). Agriculture could be especially vulnerable in northern and eastern Europe because a large share of production in the affected regions is rain-fed and irrigation infrastructure is limited. The industrial sector experiences moderate reductions (-0.75 pp on average), especially in eastern Europe and Baltic countries while manufacturing remains broadly stable (-0.11 pp on average), with pronounced impact also in these regions, which might reflect that the protective effect of indoor production environments, which buffer the output from heat waves and droughts. However, these aggregated results should be interpreted with caution, as they mask the temporal heterogeneity over the 2002–2022 period.

The paper is structured as follows: Section 2 introduces the data; Section 3 develops the construction of compound climate indicators; Section 4 details the predictive methodologies and results; Section 5 presents the design of a simulation and its outcomes; and Section 6 concludes.

2 Data Description

This study develops predictive models of sectoral GVA using economic and climate data from 1,117 NUTS-3 regions between 2002 and 2022, with economic data sourced from Eurostat. While at the time of data extraction the NUTS-3 system originally comprised 1,167 regions, economic data was unavailable for certain regions in Germany, Finland, Latvia, the Netherlands, and Portugal.[2] Although higher-frequency economic data at the national level could offer additional temporal granularity, our focus on NUTS-3 regions is deliberate. Climate shocks such as heat waves and droughts are highly localised phenomena, and their economic impacts vary significantly across regions due to differences in exposure, sectoral composition, and adaptive capacity. Aggregating to the country level would obscure these spatial heterogeneities, which are central to our research

[2] A new NUTS classification, NUTS 2024, has since been released.

question.

The economic dataset combines regional EU GVA per capita growth by sector: agriculture (A), industry aggregate excluding construction (B-E), with manufacturing (C) presented separately as a subset.[3] It also considers regional and sectoral employment-to-population ratio and country-level real GDP per capita growth, used as proxies for, respectively, the regional importance of a sector and the country's economic conditions and degree of centralised planning.

This economic data reveals significant regional disparities in economic growth during the study period, as indicated by the developments of total nominal GVA per capita (Figure A.1). In the early years of the period, regions of the Nordic countries, central Europe, northern Italy and Ireland exhibited markedly higher GVA per capita compared to most other European regions, and eastern Europe lags far behind the EU average. Over the subsequent years, eastern Europe underwent a pronounced catching-up process, narrowing much of this initial gap. In contrast, many Mediterranean regions experienced more modest growth, with several regions in Greece notably recording a decline in GVA per capita over the period.

A key contribution of the paper is the integration of climate indicators from the Copernicus European Drought Observatory. Table 1 summarises the selected variables: the Heat and Cold Waves Index (HCWI) for heat waves; the Standardised Precipitation Index (SPI) for meteorological droughts at short (SPI01), medium (SPI06), and long (SPI12) horizons; the Low-Flow Index (LFI) for hydrological droughts; and the Soil Moisture Anomaly (SMA) together with the Fraction of Absorbed Photosynthetically Active Radiation (fAPAR) for agricultural droughts.[4] The varying accumulation periods of SPI are crucial for capturing drought impacts across different timescales, with shorter periods (SPI01) indicating immediate effects like reduced soil moisture, medium periods (SPI06) reflecting streamflow and reservoir storage deficits, and longer periods (SPI12) highlighting groundwater and reservoir recharge reductions.

The climate variables capture periods of abnormal conditions relative to long-term averages. The severity of heat waves and droughts is measured using standardised indices (described in Table 1), which define threshold values for anomalous events. Specifically, heat waves and droughts are characterised by HCWI and LFI values greater than zero and SPI, SMA and fAPAR values less than or equal to -1. Consequently, the variables were coded to indicate only the occurrence

[3] GVA is expressed on a per capita basis to control for the association between regional size and population density with economic productivity, and converted to real terms using NUTS-2 deflators. Due to data limitations, NUTS-3 deflators could not be constructed.

[4] Methodological details of the indices are available at https://drought.emergency.copernicus.eu/data/factsheets/.

Table 1: Main Climate Variables

Variable	Definition	Methodological Reference
HCWI	**Heat and Cold Waves Index:** Monitors daily minimum and maximum temperatures, identifying events lasting at least three consecutive days based on percentile thresholds from a 30-year climatology.	Lavaysse et al. (2018)
SPI	**Standardised Precipitation Index:** Detects meteorological droughts and floods by measuring precipitation anomalies over accumulation periods of 1, 6, and 12 months, capturing short-term drought impacts like soil moisture deficits to long-term effects like groundwater declines. Thresholds below -1 indicate drought conditions, while values above $+1$ signal excess rainfall or potential flooding.	McKee et al. (1993)
LFI	**Low Flow Index:** Detects periods of unusually low river discharge compared to long-term thresholds, updated every 10 days. Severity is classified from low to high.	Cammalleri et al. (2017)
SMA	**Soil Moisture Anomaly:** Measures deviations in soil moisture from long-term averages, using daily data and 10-day updates. Values below -1 indicate drought stress, while values above $+1$ suggest unusually wet conditions.	De Roo et al. (2000)
fAPAR	**Fraction of Absorbed Photosynthetically Active Radiation:** Measures deviations in photosynthetic activity from long-term averages, updated every 10 days. Negative anomalies, below -1, indicate drought-related stress, while positive anomalies, above $+1$ reflect enhanced vegetation growth under wetter or favourable conditions.	Bojinski et al. (2014)

Source: Copernicus European Drought Observatory

of heat waves or droughts, while other conditions were set to zero.

The data show that most European regions have experienced an increase in the average number of annual days of heat waves (Figure A.2). Summer heat waves were already pronounced in the southern and northern regions at the beginning of the century (Russo et al., 2015). Since then, the largest increases have been observed in the Spanish Mediterranean, southern Italy, and across northern and eastern Europe. Moreover, heat wave frequency, expressed as the average number of months per year affected by at least one heat wave event (Figure A.3), has increased across most of Europe, with particularly strong increases observed in regions such as Spain and Romania. Furthermore, comparing the average HCWI scores between the first and last five years (Table A.1) of the sample backs claims that all countries now face more frequent and/or longer heat waves.

The average number of dry months per year, defined as the SPI01 values below -1, suggests a trend toward increased dryness in Europe over the past two decades (Figure A.4). Southern Spain and parts of eastern Europe were already prone to frequent dry months in 2002–2006, but the increase between 2018–2022 and the earlier period highlights growing dryness in central Europe (Cammalleri et al., 2020). Whereas regions in Finland saw early anomalies that later subsided, areas such as Germany experienced a persistent increase. Country-level SPI data across accumulation periods (Table A.1) reinforce this spatial pattern, indicating a shift toward drier conditions consistent with the intensification of meteorological drought in central Europe.

An assessment of hydrological and agricultural drought, indicated by mean LFI values greater than 0 and mean SMA figures below -1, reveals patterns similar to meteorological drought (Figures A.5 and A.6). Between 2002 and 2006, Spain, eastern Europe, and Scandinavia recorded on average up to eight hydrological and five agricultural dry months annually. From 2018 to 2022, these regions, along with parts of France and central Europe, experienced further increases, indicating increased intensity and spread of hydrological and agricultural drought conditions. In addition, fAPAR data below -1 highlight long-term trends in agricultural drought, with regions particularly in western and northern Europe showing significant increases in the number of dry months, particularly between 2013 and 2022, as compared to the previous decade (Figure A.7).

Missing climate data, excluding systematically missing values, were addressed using a targeted imputation approach within region-year groups. This method leverages the shared climatological conditions of neighbouring regions over the same period to ensure accurate and context-sensitive data reconstruction. Outliers were not removed but instead treated as valuable signals: extreme values were either incorporated into variability measures or flagged using categorical indicators, such as drought severity classes. This approach ensures that extreme events are preserved and meaningfully integrated into the analysis, rather than being excluded.

3 Calculating Compounding Indicators

We account for the compounding nature of climate events shaped by temporal and geographic factors. Temporal compounding is addressed by incorporating event duration into climate variables, so that longer events yield higher severity indices, while geographic compounding is addressed by incorporating a variable accounting for the climate conditions across neighbouring regions. Lastly, we introduce a feature to account for the coincidence of heat waves and droughts.

Localised climate shocks can trigger spillover price effects, such as the 50% increase in EU olive oil prices after droughts in Spain and Italy (Kotz et al., 2025), while heat-induced productivity losses cascade through supply chains (Sun et al., 2024). To analyse how spatially compounding heat waves and droughts are associated with GVA, we compute regional averages of climate features across neighbouring areas. For each region r, geographical compounding of a climate indicator $\mathrm{GC}^X_{t,r}$ is defined as the mean value of that indicator in neighbouring regions N_{r^*}:

$$\mathrm{GC}^X_{t,r} = \frac{1}{|N_{r^*}|} \sum_{i \in N_{r^*}} X_{t,i}, \quad \text{where } X_{t,r} \in \{\mathrm{HCWI}_{t,r}, \mathrm{SPI01}_{t,r}, \mathrm{SPI06}_{t,r}, \mathrm{SPI12}_{t,r}, \mathrm{LFI}_{t,r}\}, \qquad (1)$$

such that variables are indexed by time (t) and region (r), and $X_{t,i}$ represents the climate indicator in region i from the subset of neighbouring regions (r^*) of r. We exclude agricultural drought indicators (SMA and fAPAR) from this aggregation since, within the short- to medium-term prediction window, they exhibit minimal cross-regional compounding effects (Sepulcre-Canto et al., 2012). Geographic compounding captures shared climate systems and cross-border influences, refining regional exposure measures. Correlation analysis shows weak intercorrelations among individual indicators but strong associations (0.6–0.9) between geographic compounding variables and their respective features (X). Such multicollinearity challenges linear models but is mitigated in ML through regularisation techniques that shrink or penalise correlated coefficients.

Usman et al. (2025a) find that concurrent heat waves and droughts significantly reduce medium-term regional output, especially in less wealthy areas. Studying these compound events is essential to understand their predictive contributions. In our models, compounding is captured by variables interacting HCWI and SPI. To ensure comparability, each indicator (v) is scaled using Min-Max normalisation with a zero lower bound as follows:

$$\tilde{v}_{t,r} = \frac{v_{t,r} - \min(v)}{\max(v) - \min(v)}. \tag{2}$$

We represent heat wave and drought compounding by interacting the scaled $HCWI$ and SPI across accumulation periods $p \in \{1, 6, 12\}$. The compounding indicator $EC^p_{t,r}$ is defined as:

$$\mathrm{EC}^p_{t,r} = \begin{cases} \tilde{HCWI}_{t,r} \times \left|\tilde{SPI}^p_{t,r}\right|, & \text{if } HCWI_{t,r} > 0 \text{ and } SPI^p_{t,r} \leq -1, \\ 0, & \text{otherwise,} \end{cases} \tag{3}$$

with the indicators for each p aggregated as:

$$\mathrm{EC}_{t,r} = f_{p \in P}(\mathrm{EC}^p_{t,r}). \tag{4}$$

This formulation captures concurrent heat wave–drought events by multiplying heat stress ($HCWI$) and drought severity (SPI) across accumulation periods p. The indicator activates only when a heat wave occurs ($HCWI > 0$) along with a meteorological drought ($SPI \leq -1$). Multiple SPI periods reflect differing drought-related ecological outcomes. However, due to sparsity, indicators from all periods are combined into a single measure as shown in Equation 4. The functional form of $f_{p \in P}(\cdot)$ in Equation 4 depends on the mixed-frequency approach in Section 4.1, whereby a singular

factor is extracted from the monthly aggregates of the different $EC^{p}_{t,r}$. Coinciding events were most frequent in Mediterranean countries, primarily Italy, Spain, Cyprus and Malta, and parts of central and eastern Europe, notably Germany and Hungary, predominantly in later years.

4 Predictive Exercise

4.1 Predictive Approaches

For sector s, with variables indexed by time t, region r and country c, Equation 5 shows our benchmark economic model and Equation 6 presents the climate-augmented version. Model 5 predicts real growth in per capita GVA ($Y_{t,r,s}$) using its lag ($Y_{t-1,r,s}$), sectoral employment share ($E_{t,r,s}$), lagged country real GDP per capita growth ($G_{t-1,c}$), geographic controls (M_r, R_r, C_r), and a NUTS-3 indicator (N_r). Model 6 (f_{CLIM}) extends the economic benchmark model (f_{ECON}) with climate variables that capture heat waves, droughts, and their geographical and event compounding. Geographical compounders, $GC^{X}_{t,r}$ for $X_{t,r} \in \{\text{HCWI}_{t,r}, \text{SPI01}_{t,r}, \text{SPI06}_{t,r}, \text{SPI12}_{t,r}, \text{LFI}_{t,r}\}$, are represented by $GC_{t,r}$. Parameters and hyper-parameters are denoted by $\theta_{ECON,s}$ and $\theta_{CLIM,s}$.

$$Y_{t,r,s} = f_{ECON}(Y_{t-1,r,s}, E_{t,r,s}, G_{t-1,c}, M_r, R_r, C_r, N_r; \theta_{ECON,s}) \tag{5}$$

$$\begin{aligned} Y_{t,r,s} = f_{CLIM}(&Y_{t-1,r,s}, E_{t,r,s}, G_{t-1,c}, \text{HCWI}_{t,r}, \text{SPI01}_{t,r}, \text{SPI06}_{t,r}, \text{SPI12}_{t,r}, \\ &\text{LFI}_{t,r}, \text{SMA}_{t,r}, \text{fAPAR}_{t,r}, GC_{t,r}, EC_{t,r}, M_r, R_r, C_r, N_r; \theta_{CLIM,s}) \end{aligned} \tag{6}$$

Geographic controls identify mountainous (M_r), rural (R_r), and coastal (C_r) regions. In general, 44.0% of the regions are mixed urban–rural, 35.3% predominantly rural, 20.7% urban; 26.7% include mountain areas and 29.1% are coastal. These fixed factors influence production, connectivity, and regional heterogeneity. To capture additional heterogeneity, we encode NUTS-3 labels (N_r) using CatBoost encoding, which replaces categories with smoothed conditional means of the target, while applying Bayesian smoothing to reduce over-fitting and carefully incorporating the global mean to prevent data leakage. Encoding techniques generally outperform traditional fixed effects in predictive contexts, particularly when categories are numerous (Pargent et al., 2022). Fixed effects absorb entity-specific heterogeneity, which improves causal identification but imposes a rigid linear structure and scales poorly with high-cardinality identifiers, such as NUTS-3 regions (Wooldridge, 2010). By contrast, encoding allows us to transform categorical variables into numerical representations using an ordered scheme that prevents target leakage and enables us to capture complex nonlinear interactions between NUTS-3 regions (Prokhorenkova et al., 2018).

To reconcile the frequency mismatch between annual economic indicators and daily climate observations, we employ three mixed-frequency techniques grouped into aggregation and feature extraction approaches (Li et al., 2024) (Table 2). First, yearly aggregation summarises daily climate data into annual medians and standard deviations, capturing both central tendencies and volatility. Deviations from historical norms and intra-month variability are incorporated using the median of monthly standard deviations, following Ciccarelli et al. (2023). In this approach, geographic compounding variables are retained as distinct features from their underlying climate variables, allowing for independently calibrated weighting of geographic effects. In contrast, event-compounding indicators across different drought durations are aggregated using $f_{p\in P}(\cdot)$, as defined in Equation 4, to mitigate sparsity.

Second, feature extraction condenses high-frequency climate signals from monthly medians into interpretable annual indicators using two complementary methods: PCA and MIDAS (Table 2). The former provides an unsupervised summary of climate variation, mitigating multicollinearity by extracting a single feature per climate indicator. The latter, in contrast, applies beta-distributed lag weights to monthly observations, capturing delayed and nonlinear effects such as the gradual onset and dissipation of extreme events (Duo, 2025). Together, these approaches preserve essential climate dynamics while ensuring compatibility with annual economic models. Given the non-linear feature weighting schemes inherent to these approaches, geographic compounding variables ($GC^{X}_{t,r}$) are incorporated alongside their corresponding base indicators ($X_{t,r}$). This specification mitigates multicollinearity by extracting a single composite feature for each climate indicator. Event-based compounding indicators ($\mathrm{EC}^{p}_{t,r}$) are likewise combined using either PCA or MIDAS; accordingly, $f_{p\in P}(\cdot)$ in Equation 4 denotes the selected extraction operator, thereby reducing sparsity.

To evaluate and compare predictive performance for regional real growth in per capita GVA, we employ a linear regression benchmark (Martín Cervantes et al., 2020; Kahn et al., 2021; Mohaddes et al., 2023) alongside two tree-based ML models: Random Forest and XGBoost. All models are trained on data up to 2017 and assessed out-of-sample for the period 2018 to 2022. Ensemble methods are particularly well suited for this task as they capture nonlinearities and complex interactions between climate and economic variables (Rossi et al., 2023).

Random Forest constructs an ensemble of decision trees using bootstrapped samples and introduces randomness by selecting subsets of predictors at each split. Predictions are obtained by averaging across trees, which reduces variance and mitigates over-fitting in the presence of collinear climate indicators, while also providing interpretable measures of variable importance (Breiman,

Table 2: Treatment of Climate Variables in Engineering Pipelines

Variable	Compounding	Aggregations	PCA	MIDAS
$HCWI_{t,r}$	Temporal & Geographic	$\bar{HCWI}$, $\bar{GC}$ σ^{HCWI}, σ^{GC}	$\tilde{HCWI} = f^{PCA}(HCWI, GC)$	$\tilde{HCWI} = f^{MIDAS}(HCWI, GC)$
$SPI01_{t,r}$	Temporal & Geographic	$\bar{SPI}01$, $\bar{GC}$ σ^{SPI01}, σ^{GC}	$\tilde{SPI}01 = f^{PCA}(SPI01, GC)$	$\tilde{SPI}01 = f^{MIDAS}(SPI01, GC)$
$SPI06_{t,r}$	Temporal & Geographic	$\bar{SPI}06$, $\bar{GC}$ σ^{SPI06}, σ^{GC}	$\tilde{SPI}06 = f^{PCA}(SPI06, GC)$	$\tilde{SPI}06 = f^{MIDAS}(SPI06, GC)$
$SPI12_{t,r}$	Temporal & Geographic	$\bar{SPI}12$, $\bar{GC}$ σ^{SPI12}, σ^{GC}	$\tilde{SPI}12 = f^{PCA}(SPI12, GC)$	$\tilde{SPI}12 = f^{MIDAS}(SPI12, GC)$
$LFI_{t,r}$	Temporal & Geographic	$\bar{LFI}$, $\bar{GC}$ σ^{LFI}, σ^{GC}	$\tilde{LFI} = f^{PCA}(LFI, GC)$	$\tilde{LFI} = f^{MIDAS}(LFI, GC)$
$SMA_{t,r}$	Temporal	$\bar{SMA}$, σ^{SMA}	$\tilde{SMA} = f^{PCA}(SMA)$	$\tilde{SMA} = f^{MIDAS}(SMA)$
$fAPAR_{t,r}$	Temporal	$\bar{fAPAR}$, σ^{fAPAR}	$\tilde{fAPAR} = f^{PCA}(fAPAR)$	$\tilde{fAPAR} = f^{MIDAS}(fAPAR)$
$EC_{t,r}$	Event	$\bar{EC}$, σ^{EC}	$\tilde{EC} = f^{PCA}(EC^p)$	$\tilde{EC} = f^{MIDAS}(EC^p)$

Note: The above table summarises the treatment of climate variables within the three distinct feature engineering pipelines. The Aggregations column displays the transformation of climate features and their geographic compounders, where relevant, into yearly medians ($\bar{X}$) and standard deviations (σ^X). The PCA and MIDAS columns shows that the functional forms f^{PCA} and f^{MIDAS} are used to extract a singular yearly feature ($\tilde{X}$) from the higher frequency climate features, geographic compounders, and/or accumulation periods, depending on the climate variable.

2001). In contrast, XGBoost builds trees sequentially, correcting residuals from previous iterations. Enhancing gradient boosting through second-order gradient optimisation and regularisation, making it effective for modelling nonlinear climate–economic dynamics (Chen and Guestrin, 2016).

We tuned model hyper-parameters using Optuna by minimising the average root mean squared error (RMSE) across panel-aware cross-validation folds. The optimisation jointly adjusts preprocessing, primarily K Nearest-Neighbours imputation and feature extraction, and model-specific parameters for Random Forest and XGBoost. For each trial, the pipeline is fitted to the training folds and evaluated to prevent leakage. The search spaces include the number of neighbours for imputations, tree depth and sampling parameters for ensemble methods, learning rates and regularisation terms for boosting algorithms, and beta-polynomial parameters for MIDAS-based feature extraction. We allow up to a thousand trials with early stopping after a hundred trials without improvement in the best RMSE. Upon termination, the pipeline is refitted on the full training set using the best hyper-parameters. This procedure ensures reproducibility, avoids look-ahead bias, and provides a robust framework for tuning models in panel data settings.

To generate predictions for the models represented by Equations 5 and 6, we implement an expanding rolling-window procedure that mimics sequential information arrival. The approach

begins with an initial training sample and sequentially expands the estimation window as new observations become available. For each target year, the model is re-estimated using all information available up to that point to produce out-of-sample predictions for the current period, ensuring that predictions rely only on contemporaneously available data. Model performance is evaluated using RMSE for each horizon and aggregated across all out-of-sample predictions. This expanding-window strategy captures evolving dynamics and allows for an assessment of predictive accuracy under realistic sequential learning conditions. To test whether differences in predictive accuracy between models are statistically significant, we apply a Diebold–Mariano test adapted for our panel-based predictions (Diebold, 2012).

To interpret model predictions, we employ SHAP (SHapley Additive exPlanations) values and factor loadings to identify the most influential predictors, with particular attention to climate variables affecting sectoral real growth in per capita GVA. SHAP values provide a theoretically grounded approach based on cooperative game theory, ensuring fair attribution of each feature's contribution between all possible combinations of predictors. This method offers transparent and consistent insights into model behaviour, enhancing interpretability in complex, nonlinear settings (Shapley, 1953; Lundberg et al., 2018). Importantly, these values are used solely to assess predictive contributions, rather than to infer structural relationships or establish causality.

4.2 Prediction Results

Table 3 reports the RMSEs of our predictive exercise, highlighting clear differences between linear benchmarks and ML models across sectors. Predictive ability tests indicate that climate-augmented linear models did not significantly outperform the economic benchmark (f_{ECON}) in any sector, whereas ML models exhibit sector-specific gains. For agriculture, climate-augmented ML models significantly improved accuracy over f_{ECON}, primarily driven by heat wave and drought indicators. In contrast, climate-augmented specifications (f_{CLIM}) failed to surpass f_{ECON} for sectors B–E and C within the same model class. However, ML predictions for B–E significantly outperformed all linear counterparts, while most ML predictions for sector C showed limited improvement.

Among the climate-augmented models, the simpler approach of aggregating climate variables into annual medians and standard deviations performs at least as well as, and often better than, the more complex feature-extraction techniques based on PCA and MIDAS. As shown in Table 3, this specification generally yields the most accurate climate-augmented predictions of real growth in per capita GVA, particularly in agriculture, where it significantly outperforms both the corresponding

Table 3: Predictions' RMSEs

Model	Linear Regression			Random Forest			XGBoost		
	A	B–E	C	A	B–E	C	A	B–E	C
Economic (f_{ECON})	21.64	14.11	77.90	23.05	13.83†	72.81	28.15	13.89†	76.73†
Climate (f_{CLIM})									
- Medians & St. Deviations	22.12	14.20	77.95	20.93*†§	14.01†	73.64	20.54*†§	13.95†	77.69
- PCA Features	22.23	14.17	77.91	21.05*†	13.94†	74.03	21.52*†	14.03†	77.80
- MIDAS Features	22.98	14.36	78.03	21.18*†	14.06†	75.19	21.72*†	13.97†	85.34

Note: The reported RMSEs represents the aggregate out-of-sample predictive error, evaluated across all horizons using recursively generated expanding-window year ahead predictions and observed outcomes. RMSEs are calculated over annual predictions of real growth in per capita GVA from 2018 to 2022. Sector A covers agriculture; B–E includes mining (B), manufacturing (C), utilities (D), and waste management (E), with C also modelled separately to obtain direct predictions for manufacturing. Symbols denote statistically significant improvements in predictive performance as:
* $p < 0.05$ indicates predictive improvements relative to the respective economic counterpart of the same model type;
† $p < 0.05$ indicates predictive improvements relative to the respective linear regression counterpart; and
$\S$ $p < 0.05$ indicates predictive improvements relative to the respective linear economic model for the same sector.

economic-only model and the linear regression benchmark. The simplicity of aggregating climate variables reduces model complexity and limits the risk of over-fitting, making this approach particularly robust in panels with short time spans. By contrast, feature-extraction techniques such as PCA and MIDAS introduce additional parameters and transformations, which increase over-fitting risks. However, these methods offer advantages in handling multicollinearity and preserving high-frequency patterns, enabling models to capture more nuanced temporal dynamics that simple aggregation may overlook.

A disaggregation of the RMSE scores by year for the evaluation period (Table A.2) indicates how temporal patterns further highlight the interaction between macroeconomic shocks and climate dynamics. In 2021, extreme prediction errors in manufacturing are observed that point to a pronounced structural break associated with the post-pandemic rebound, characterised by abrupt demand recovery, global supply chain bottlenecks, and energy market disruptions (Guerrieri et al., 2022). These factors introduced nonlinear and regime-dependent dynamics that are not well captured by standard economic indicators or climate variables within the training sample, leading to a systematic deterioration in predictive accuracy across all model classes. This episode underscores the limitations of conventional predictive frameworks in the presence of large, synchronised macroeconomic shocks that dominate the underlying structural relationships. Additionally, in 2022, marked by severe and spatially widespread heat waves and drought conditions throughout Europe (Toreti et al., 2022), prediction errors increase notably in agriculture, reflecting a greater sensitivity to extreme climatic stressors such as prolonged soil moisture deficits and elevated temperature

anomalies. These conditions adversely affected crop yields, water availability, and agricultural productivity more broadly, thereby amplifying volatility in Sector A. In contrast, RMSEs in industry (sector B-E) remain comparatively stable, suggesting that climate impacts in these sectors are more indirect. Nevertheless, despite the observed variation in predictive performance over the entire evaluation period, a robustness check restricted to the pre-pandemic subsample (Table A.3) indicates that the results of the predictive ability tests remain robust.

Our research then asks which factors drive predictive performance in climate-augmented models. Existing evidence suggests that economic variables typically dominate predictions, while climate indicators provide additional but context-dependent contributions (Dell et al., 2014). Our analysis of SHAP values (Tables A.4 to A.11) is consistent with this pattern: economic variables remain the strongest predictors, yet climate and geographic factors also matter, with their influence varying by sector and specification. HCWI, which includes yearly median, standard deviation, and geographic compounding for the Medians & St. Deviations version of f_{CLIM}, and extracted features for PCA- and MIDAS-based implementations, consistently emerges as a key climate indicator, while drought measures show sector-specific relevance. Heat wave indicators and short- to medium-term meteorological drought (SPI01, SPI06) dominate in agriculture, whereas in sectors B–E and C, heat waves retain importance but drought effects shift toward hydrological and long-term measures (LFI, SPI12). These findings highlight sectoral heterogeneity and demonstrate how ML models leverage regularisation to adjust feature weights, improving climate-augmented performance relative to linear benchmarks. The prominence of heat waves aligns with prior evidence of strong short-term effects (Usman et al., 2025a), while drought indicators reflect medium- to long-term dynamics.

Given the heterogeneity within our spatially granular data, we also investigate how heat waves, droughts, and their interactions influence outcomes across different regions. Prior evidence suggests that climate shocks have asymmetric effects, with droughts causing persistent losses in low-income areas and heat waves occasionally benefiting higher-income regions (Usman et al., 2025b). Our analysis using SHAP values (Tables A.6 to A.11) reveals strong regional heterogeneity: heat waves affect both high- and low-GVA regions, which are defined by a time-invariant distribution of real growth in per capita GVA, with low (high) regions below (above) the midpoint. Interestingly, heat waves sometimes benefit higher-GVA areas, while droughts disproportionately harm lower-GVA regions. Climate-related predictive contributions are more pronounced in below-median GVA regions, underscoring their vulnerability. These findings indicate that ML models capture asymmetric climate impacts, reinforcing the interpretation that climate shocks exacerbate regional disparities,

with heat waves linked to short-term gains in some high-GVA regions and droughts driving medium- to long-term losses in low-GVA regions.

When assessing whether geographic compounding indicators influence predicted outcomes and what dynamics they reveal, existing literature shows that climate-induced economic effects vary significantly across regions, with some benefiting from neighbouring disruptions due to trade and sectoral shifts, while others suffer compound losses (Dellink et al., 2019). Our analysis of SHAP values and factor loadings aligns with existing literature by suggesting that geographic compounding indicators exert a pronounced influence on predictions, reflecting both competitive and complementary dynamics (Tables A.12 to A.14). Regions often exhibit beneficial associations when neighbours experience heat waves, consistent with competitive effects, while the contributions of hydrological drought are mixed, suggesting complementarity shaped by geography and trade routes, with competitive behaviours emerging when drought conditions force deviations from established routes. These findings underscore the importance of spatial interdependencies and support the interpretation that climate shocks propagate through integrated ecological–economic systems, amplifying or mitigating regional vulnerabilities.

Our framework also allows for the analysis of compound climate events, specifically the interplay between heat waves and droughts, that affect predictive outcomes across sectors. Existing evidence suggests that climate risks exhibit nonlinear, sector-specific economic effects and that compound events often diverge from additive impacts (Zhu and Li, 2024; Yin and Slater, 2023). Our findings are consistent with this complexity: SHAP values and factor loadings (Tables A.6 to A.14) indicate that under the Medians & Standard Deviations specification of f_{CLIM}, which weights drought horizons equally, the joint contribution of heat waves and droughts is generally more negative than or equal to the sum of their individual effects. In contrast, feature-extraction approaches produce more diverse patterns, where agricultural predictions are driven by short-term droughts, while the industry aggregate (sectors B–E) and sector C respond more strongly to long-term droughts. This reflects sectoral sensitivities, where agriculture reacts to immediate vegetation stress, whereas industry is more affected by prolonged water scarcity. These results underscore the need for models that capture nonlinear and sector-specific dynamics, as compound climate shocks do not behave additively and can amplify or offset individual effects.

Lastly, we ask whether mixed-frequency feature extraction techniques reveal seasonal differences in the predictive contributions of climate indicators (Tables A.15 and A.16)[5]. Previous findings

[5]PCA assigns seasonal factor loadings consistently across models and sectors because its loadings, derived from

suggest that European summer extremes, particularly heat waves and droughts, are predictable in seasonal lead times and exert strong impacts on health, energy and agriculture (Zscheischler and Fischer, 2020; Seneviratne et al., 2021), while drought typologies indicate varying seasonal relevance for short- and long-term events (Hao et al., 2018). Our findings align with these patterns: across PCA- and MIDAS-based models, heat waves and droughts occurring in summer exhibit the strongest predictive influence, especially for heat wave indices (HCWI) and event-compounding indicators (EC). Beyond summer, short- to medium-term meteorological droughts (SPI01, SPI06) contribute more in spring and autumn, while long-term and hydrological droughts (SPI12, LFI) peak in spring, reflecting hydrological memory and basin-scale water deficits. Agricultural droughts emerge as outliers, with predictive signals concentrated in cooler seasons, primarily winter but also spring and autumn, consistent with agricultural drought diagnostics (European Commission Joint Research Centre, 2025). These results underscore the importance of seasonality and compound-event dynamics in climate-sensitive sectors and highlight the value of mixed-frequency approaches to reflect temporal nuances.

Although the SHAP-based feature importance analysis clarifies which predictors most strongly contribute to the model's predictions, these results should be interpreted as conditional associations rather than causal effects. While our analysis aligns with the referenced literature, SHAP magnitudes reflect the model's learned relationships under the observed covariate distribution, and can be influenced by collinearity, interaction structure, and specification choices; consequently, importance can be distributed across correlated features and need not imply directionality or policy-relevant impact. Establishing causality would require an explicit identification strategy, along with diagnostics and robustness checks tailored to those designs. Accordingly, we refrain from causal claims here and view the SHAP results as informative for model interpretability and an assessment of the models' alignment with the existing literature.

the correlation matrix eigensystem, remain fixed. In contrast, MIDAS estimates lag-weight functions through hyper-parameter tuning, which optimises polynomial weights for the training data and prediction horizon, causing seasonal importance to vary by model. Consequently, MIDAS can exhibit model-specific seasonality, whereas PCA maintains stable seasonal rankings per climate feature. Overall, seasonal predictive importance across climate features remains broadly aligned between PCA- and MIDAS-based feature extraction techniques.

5 Application: A Simulation of Extreme Compound Events

5.1 Simulation Design

To further examine the influence of heat waves and droughts on real growth in per capita GVA, we design a comparative analysis of two distinct scenarios: the non-event and 2022-based event scenarios. We adopt 2022 as the benchmark year, as it represents the period most severely affected by concurrent heat waves and droughts in our sample, as documented by Tripathy and Mishra (2023). These simulations are estimated using XGBoost with the yearly aggregation approach, selected for its consistently superior performance in minimising RMSEs across climate-augmented models, as detailed in Section 4.2.

The non-event scenario is defined as a counterfactual benchmark in which all climate variables are set to zero, while economic covariates and geographic controls are held fixed at their observed values. The constructed set of climate variables ($\mathcal{V}$) to reflect our non-event scenario is denoted by $D^{\dagger}$, as described by Equation 7. This configuration represents the absence of heat wave and drought conditions:

$$\begin{aligned} \mathcal{D}^{\dagger} &= \{(v, 0) : v \in \mathcal{V}\} \quad \text{with} \\ \mathcal{V} &= \{\text{SPI01}, \text{SPI06}, \text{SPI12}, \text{SMA}, \text{fAPAR}, \text{HWCI}, \text{LFI}, \text{EC}, \sigma\}, \end{aligned} \tag{7}$$

where the variables SPI01, SPI06, SPI12, HCWI and LFI in set $\mathcal{V}$ represent both indicators for a region's own mean or median climate conditions and their geographic compounders, while σ denotes the set of standard-deviation for each $v \in \mathcal{V}$.

The 2022 event scenario dataset of climate variables, denoted by $\mathcal{D}^{\gamma^*}$ (where γ is 2022) and described in Equation 8, simulates extreme climate conditions based on extreme heat wave events and agricultural, meteorological, and hydrological droughts observed in 2022. Economic covariates and geographic controls are again held fixed at their observed values, but each climate variable is replaced with its relevant tail percentile drawn from the pooled 2022 distribution, such that:

$$\begin{aligned} \mathcal{D}^{\gamma^*} &= \left\{ \left(v, Q_{\tau(v)}(\{v_{t,r} : t \ = \gamma\}) \right) : v \in \mathcal{V} \right\}, \text{with} \\ \tau(v) &= \begin{cases} 0.01, & v \in \{\text{SPI01}, \text{SPI06}, \text{SPI12}, \text{SMA}, \text{fAPAR}\}, \\ 0.99, & v \in \{\text{HWCI}, \text{LFI}, \text{EC}, \sigma\}, \end{cases} \end{aligned} \tag{8}$$

where $Q_{\tau(v)}$ represents the tail percentile function. The first percentile of SPI01, SPI06, SPI12, SMA, and fAPAR, and the ninety-ninth percentile of HCWI, LFI, the compound-effect index EC, and the standard deviation measures σ are used to capture extreme climate conditions, in line with the distributional properties of each variable as reported in Table 1. The percentile thresholds applied to geographic compounders are in line with the thresholds applied to the indicators for a region's own climate conditions.

As a robustness check, we also construct an alternative event scenario, denoted by $\mathcal{D}^{**}$ and described in Equation 9, in which the same variable-specific tail assignments are preserved, but the corresponding percentiles are computed from the pooled distribution over the full 2002–2022 period rather than from 2022 alone:

$$\mathcal{D}^{**} = \left\{ \left(v, Q_{\tau(v)}(\{v_{t,r} : t \in [2002, 2022]\}) \right) : v \in \mathcal{V} \right\}. \tag{9}$$

Pooling across all regions yields thresholds that are comparable in terms of extremeness, irrespective of local climate regimes. As shown in Figure A.8 in the Appendix, the RMSE between $\mathcal{D}^{\gamma^*}$ and $\mathcal{D}^{**}$ attains its minimum in 2022. Given that each climate index is standardised with respect to the long-term climatological average of the respective region, hence, fixing a variable at its extreme percentile imposes the same standardised deviation from the mean in every region. This ensures a uniform level of climatic stress across regions and allows the estimated economic effects to be interpreted as responses to an equally severe climatic shock in each NUTS-3 location.

The predicted real growth in GVA per capita under the event and non-event scenarios are denoted by $\hat{y}^{*}_{t,r,s}$ and $\hat{y}^{\dagger}_{t,r,s}$, respectively. The simulated effect of the extreme compounding heat wave and drought events on $Y_{t,r,s}$ is calculated as the difference between these predictions:

$$\Delta\hat{y}_{t,r,s} = \hat{y}^{*}_{t,r,s} - \hat{y}^{\dagger}_{t,r,s}. \tag{10}$$

In the illustrative exercise of the next section, all regions are assumed to be uniformly exposed across time to climatic conditions comparable to those observed in 2022. The resulting economic impacts by NUTS-3 region and sector $\overline{\Delta\hat{y}}_{r,s}$ is defined by Equation 11.

$$\overline{\Delta\hat{y}_{r,s}} = \frac{1}{T} \sum_{t=2002}^{2022} \Delta\hat{y}_{t,r,s} \tag{11}$$

5.2 Simulated Outcomes

The outcomes of the simulation for agriculture, depicted in Figure 1, show that the EU's agriculture would experience widespread negative contributions from a heat wave and drought event similar to 2022. We find that 99% of regions would experience losses ranging from −7.36 to −1.93 pp in real per capita GVA growth[6], indicating substantial regional heterogeneity. Eastern Europe, especially Romania, Czech Republic, Bulgaria, Slovenia and Croatia, faces the most severe simulated losses (−5.36 pp on average), while western regions, such as Germany and France, experience less severe simulated consequences (−4.4 pp on average)[7]. Southern Europe experiences moderate negative outcomes in Greece and Italy, with on average −3.9 pp losses.

Agricultural adaptive capacity and irrigation systems may help explain these results. Although southern Europe is characterised by chronic drought, heat stress, soil erosion, and water scarcity (European Environment Agency, 2026), the comparatively smaller estimated impacts on agricultural GVA may reflect structural adaptation to persistent climatic stress rather than lower exposure. In this regard, Vanschoenwinkel et al. (2016) document higher agricultural adaptive capacity to climate change in western Europe relative to eastern Europe. Similarly, Lesk et al. (2022) and Tabari and Willems (2023) show that agricultural systems in cooler, traditionally less drought-adapted regions may be more sensitive to compound extreme events, potentially due to lower baseline resilience to simultaneous heat and water stress.

In southern Europe, the widespread use of irrigated agriculture can partially buffer short-run output losses associated with drought and heat stress, thereby attenuating climate signals in aggregate agricultural GVA except during extreme events. However, recent episodes of irrigation water restrictions highlight that this buffering capacity is finite and contingent on water availability (Toreti et al., 2022). By contrast, eastern and northern European regions rely more heavily on rain-fed agriculture and have less developed irrigation infrastructure (Zajac et al., 2022), exposing agricultural production more directly to drought conditions and generating stronger short-run output responses. This interpretation aligns with documented regional heterogeneity in irrigation coverage and climate vulnerability, as well as evidence that the frequency and intensity of drought events in Europe have increased in recent years (Rossi et al., 2023). This trend suggests that irrigation-based adaptation may become progressively less effective under future climate conditions.

[6] Minimum and maximum values are −10.96 (NUTS-3 region: BE100) and −1.23 pp (NUTS-3 region: EL305), respectively.

[7] We follow the geographical classification of EuroVoc (Publications Office of the European Union, 2026).

Figure 1: Simulation of the Average Effects of a Heat Waves & Droughts on Sector A

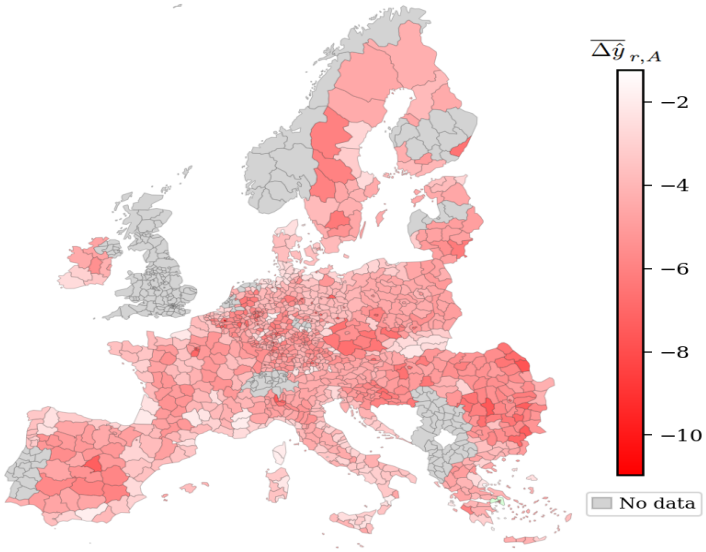

Note: The figure illustrates the difference between the event and non-event scenarios, as defined in Equations 10 and 11, for the agricultural sector (A). Values are reported using a colour scale ranging from zero (white) to minus eleven pp (red). Simulated outcomes are not available for regions in Germany, Finland, Latvia, the Netherlands, and Portugal (shown in grey) due to the unavailability of underlying economic data at the time of data collection.
Source: Authors' calculations

Figure 2 shows that the simulated effects on industry (left) and manufacturing (right) are predominantly negative, but considerably less severe and less spatially widespread than in agriculture.

For the broader industrial sector (B–E), including utilities and energy, results indicate moderate but spatially heterogeneous negative effects across the EU, with 99% of the NUTS-3 regions experiencing reductions in real per capita GVA growth of 0–2 pp[8] under the 2022 event scenario. Negative effects are more visible in eastern Europe, especially in Bulgaria, Poland, Romania, Slovakia, Hungary, Czech republic and Croatia (−1.39 pp on average), and the Baltic countries (−1.18 pp on average), highlighting that economically emerging European countries within the EU are more vulnerable to the impacts of extreme heat and droughts (Mátyás, 2022).

The right panel of Figure 2 shows that manufacturing (C) is substantially less affected by our 2022 based heat wave and drought scenario than the broader industrial aggregate. Across most of the EU, simulated losses in real per capita GVA growth remain close to zero and generally do not exceed −0.36 pp for 99% of the regions[9]. Negative effects are more visible in Baltic countries with average losses of −0.33 pp and eastern regions, in particular in Bulgaria, Romania, Croatia,

[8]Maximum and minimum values are respectively 0.11 pp (NUTS-3 region: ITI1A) and −3.28 pp (NUTS-3 region: ITG19). Positive values occur in six regions in France (out of 96 NUTS-3 regions), six regions in Italy (out of 107 NUTS-3 regions) and one in Belgium (out of 44 NUTS-3 regions).

[9]Maximum and minimum values are respectively 0.23 pp (NUTS-3 region: BE329) and −0.40 pp (NUTS-3 region: LT023). Positive values occur in nine regions in Belgium (out of 44 NUTS-3 regions), four regions in Italy (out of 107 NUTS-3 regions), two in Germany (out of 394 NUTS-3 regions) and one in Spain (out of 51 NUTS-3 regions).

Figure 2: Simulation of Heat Waves and Droughts on Sectoral Aggregates B-E (left) & C (right)

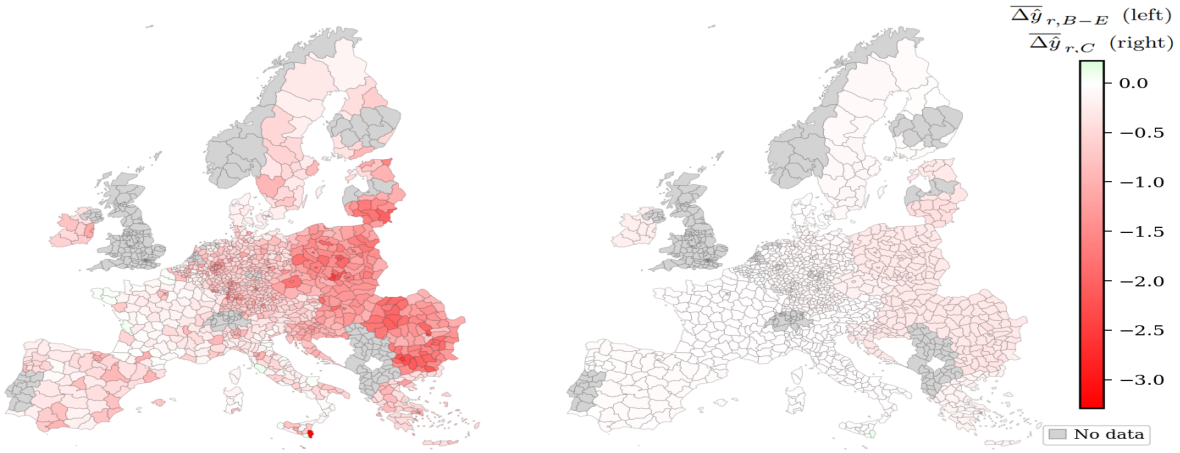

Note: The figure illustrates the difference between the event and non-event scenarios, as defined in Equations 10 and 11, for the industrial (B-E, left) and manufacturing (C, right) sectors. Values are reported using a colour scale ranging from positive (green) to negative (red). Simulated outcomes are unavailable for regions in Germany, Finland, Latvia, the Netherlands, and Portugal because the underlying economic data were unavailable at the time of collection.
Source: Authors' calculations

Hungary, Slovakia and Poland, with average losses of −0.30 pp.

This relative resilience of the manufacturing sector compared to the industrial aggregate can reflect the prevalence of controlled indoor production environments. Indeed, according to García-León et al. (2021), heat waves can largely reduce GVA through labour productivity losses concentrated in outdoor activities. Since manufacturing is predominantly indoor, its direct vulnerability to heat appears relatively limited. By contrast, the broader industrial aggregate includes activities with greater outdoor or infrastructure-related exposure such as extraction or water infrastructure, which can lead to larger losses.

Nevertheless, these relatively modest estimated impacts require further contextualisation. As depicted on Table A.17 in the Appendix, according to Eurostat data, manufacturing accounted on average for 16.9% of EU GVA over the period considered, while industry excluding construction and manufacturing represented 3.15%, and agriculture, forestry and fishing 1.89%. Therefore, even small percentage declines in manufacturing can translate into economically significant absolute losses, given the sector's much larger weight in the EU economy.

To complement the simulation results, Figure A.9 reports country-level intermediate consumption of energy products (ICNS) by sector from 2002 to 2022 (Eurostat, 2024) to study the relation between our results and energy-intensive sectors. The ICNS measure captures the use of energy products as intermediate inputs into production, and therefore provides a direct proxy for the extent

to which different sectors and countries rely on energy in their productive activities. Agriculture accounts for a small share of ICNS (2.3%) but exhibits the largest GVA declines, indicating that its vulnerability is mainly driven by direct exposure to heat and drought. By contrast, manufacturing accounts for the largest share of ICNS (65.3%) and contains subsectors classified by the European Commission as Energy-Intensive Industries[10] (European Commission, 2021), notably coke and petroleum (C19), chemicals (C20), non-metallic minerals (C23), basic metals (C24), paper (C17), and wood (C16), but shows comparatively limited effects. Lastly, the industry without manufacturing (B, D, and E) occupies an intermediate position. Overall, these results suggest that climatic exposure and sectoral sensitivity matter more than energy-product use alone.

The stronger sensitivities observed in parts of eastern Europe may reflect the interaction between industrial structure, energy-system characteristics and climate-sensitive infrastructure. Eastern European countries follow heterogeneous energy-transition pathways, with varying degrees of fossil-fuel dependence, nuclear reliance, renewables deployment, energy intensity and import exposure (Guarascio et al., 2025; Nichifor et al., 2025; Santa et al., 2025). Relative to many western European regions, parts of eastern and southeastern Europe may be more vulnerable in regions where rapid industrial integration coincides with higher energy intensity, ageing energy and water infrastructure, and uneven adaptive capacity. This may amplify drought and heat wave shocks through pressure on power generation, cooling-water availability, infrastructure reliability and energy-intensive production.

As a robustness check, the simulation results remain largely unchanged when percentiles are computed over the full 2002–2022 period rather than from 2022 alone, as shown in Figure A.10 for sector A and Figure A.11 for sectors B–E and C. It is important to note, however, that the reported results represent averages across all years and therefore mask substantial temporal heterogeneity. As illustrated in Figure A.12, which shows the yearly dispersion across NUTS-3 regions, the simulated 2022 heat wave and drought effects vary considerably over time, with the greatest dispersion observed in agriculture, followed by industry and manufacturing, in line with the aggregated patterns. This variation reflects differences in the underlying economic environment as well as the non-linear structure of the XGBoost model. Consequently, estimates for periods such as the post-financial crisis and post-COVID years are influenced by exceptional macroeconomic conditions and should be interpreted with caution.

[10]Sectors with above-median energy input cost shares in total input costs in the EU.

6 Conclusions

This study investigates how heat waves and droughts play a role in shaping regional and sectoral output in the EU and proposes climate-augmented predictive models to assess these effects in real time. Our results suggest that heat and dryness exert material, nonlinear, and sector-dependent predictive influences on regional economic activity. In climate-sensitive sectors, ML-based predictions reflect these interactions more effectively than linear benchmarks, which aligns with recent European assessments that highlight the importance of nonlinear intensifications and seasonality of heat and drought signals (Ionita et al., 2021).

Across models and indicators, the highest predictive gains arise in agriculture, where heat wave and drought indicators of ML models improve accuracy compared to the economic-only baselines and linear benchmarks. The results suggest that, although alternative sectoral aggregations yield modest improvements in predictive performance when using the ML models, specifications augmented with climate variables do not significantly outperform their purely economic benchmark counterparts. In our approximately 20-year panel, the annual aggregation (medians and standard deviations) of higher frequency climate variables yields predictions that are at least as accurate and often more robust than PCA- and MIDAS-based feature extraction. This finding is consistent with PCA stability and interpretability issues in short time-series, with additional evidence that mixed-frequency models can be sensitive to limited samples (Zhang and Tong, 2022; Kuzin et al., 2011). SHAP-based feature-importance analysis highlights that, after economic predictors, heat wave indicators remain the dominant predictors, while drought types and horizons contribute in a sector-specific manner, such that agricultural and short-to-medium horizons contribute more to agricultural predictions, and hydrological and longer horizons have a role in industry outcomes, echoing European evidence on heat and drought related economic stress (Dell et al., 2014; Usman et al., 2025a).

Scenario analyses based on the XGBoost model that achieved the lowest RMSEs in our predictive exercise show that compound heat wave and drought conditions similar to those experienced in 2022 generate the most pronounced output losses in agriculture. Relative to a no-anomaly climate benchmark, the simulated event reduces real per capita GVA growth in agriculture by an average of 4.54 pp, and losses are concentrated in eastern Europe, where adaptive capacity to heat waves and droughts are less developed (Vanschoenwinkel et al., 2016) while southern Europe experiences milder losses, reflecting the buffering effect of more extensive irrigated systems (Toreti et al., 2022).

The industrial sector exhibits moderate, spatially heterogeneous declines, averaging −0.75 pp. The strongest effects are again observed in eastern Europe and the Baltic states. By contrast, manufacturing remains comparatively more resilient than the broader industry, with an average loss of -0.11 pp. This relative stability likely stems from the predominance of indoor production environments that limit direct exposure to extreme heat, as well as from the sector's lower reliance on outdoor, climate-sensitive activities compared with the broader industrial aggregate (García-León et al., 2021). The stronger sensitivities observed in parts of eastern Europe may also reflect the interaction between industrial structure, energy-system characteristics and climate-sensitive infrastructure (Guarascio et al., 2025; Nichifor et al., 2025; Santa et al., 2025). Although the main results are robust to computing percentiles over the full 2002–2022 period, the estimates should be interpreted with caution because averaging across years mask temporal heterogeneity.

These findings refine climate–economy links by emphasising heterogeneity, nonlinearity and spatial interdependence; geographically compounding signals and regional interdependence are consistent with spatial-economic spillovers (Dellink et al., 2019). Methodologically, climate-augmented mixed-frequency predictive modelling adds value to real-time assessments, complementing established approaches while capturing interactions that linear models often miss, and provides the ability to target climate-event scenarios for specific seasons or months. From a policy perspective, improvements in climate-augmented predictive modelling can underpin early-warning systems, inform regional fiscal planning (e.g., contingency funds and intergovernmental transfers), and guide adaptation policy by identifying where and when heat wave and drought events are most likely to impair sectoral output.

Nevertheless, the scope of these conclusions is EU NUTS-3 regions over 2002–2022 are conditioned on our modelling design and choice of indicators. Several limitations warrant caution. First, we emphasise predictive accuracy, rather than causal identification, where SHAP-based interpretability captures conditional associations, not structural parameters (Lundberg et al., 2018). Second, simulations impose a uniform extreme shock across regions, simplifying heterogeneous local hazards and compounding pathways documented for Europe (Ionita et al., 2021). Third, spatial and temporal autocorrelations of climate events can create clustered patterns that complicate attribution of observed effects. Finally, some regions are excluded due to data limitations, and the relatively short evaluation period, which encompasses the COVID-19 pandemic, constrains the stability of the modelling techniques, such as the high-dimensional feature extraction.

Future work should integrate additional compounding hazards, seasonal variables, and adapt-

ation indicators, test external validity beyond the EU and into services, link real-time prices and supply-chain channels to output predictions, and explore causal ML and econometric identification to isolate mechanisms to then couple sectoral predictions with financial-exposure data for system-wide stress testing under richer scenario sets. Additionally, future modelling efforts may need to integrate more absolute heat and water-availability thresholds particularly those relevant for cooling constraints, process water requirements, and regulatory shutdowns, to better characterise nonlinear impacts in manufacturing and energy-intensive activities. Progress in these directions would align the empirical strategy with emerging European climate intelligence and supervisory priorities (Usman et al., 2025b; Kotz et al., 2025; Ceglar et al., 2025).

Longer-duration drought indicators should also be explored, as multi-season or multi-year droughts are more directly linked to water supply constraints affecting irrigation reservoirs, river discharge for cooling, and industrial water abstraction. Additionally, compound-event analysis should be broadened beyond the most extreme heat wave and drought episodes to include combinations of moderately adverse heat and drought conditions. Evidence from the compound-risk literature suggests that materially adverse impacts can arise even when individual hazards are not extreme, due to interaction and amplification mechanisms (Zscheischler and Fischer, 2020; Ceglar et al., 2025). Capturing such effects would improve the realism of scenario narratives design and enhance the relevance of predictions for anticipatory policy and risk management.

Our results advance a practical and interpretable approach to real-time climate–economic predictive exercises. By quantifying where compound heat wave and drought events are most likely to depress regional sectoral output, the predictive models offer an evidence base for targeted adaptation and economic-stability analysis across the EU.

References

Baruth, B., Bassu, S., Ben Aoun, W., Biavetti, I., Bratu, M., Cerrani, I., Chemin, Y., Claverie, M., De Palma, P., Fumagalli, D., Manfron, G., Morel, J., Nisini Scacchiafichi, L., Panarello, L., Ronchetti, G., Seguini, L., Tarnavsky, E., Van den Berg, M., Zajac, Z., and Zucchini, A. (2022). JRC MARS Bulletin – Crop Monitoring in Europe. *Publications Office of the European Union, Luxembourg*, 30(6).

Battiston, S., Monasterolo, I., van Ruijven, B., and Krey, V. (2022). The NACE – CPRS – IAM mapping: A tool to support climate risk analysis of financial portfolio using NGFS scenarios. *SSRN*. Available at SSRN: https://pure.iiasa.ac.at/id/eprint/18530/1/SSRN-id4223606.pdf.

Beirne, J., Dafermos, Y., Kriwoluzky, A., Renzhi, N., Volz, U., and Wittich, J. (2021). The Effects of Natural Disasters on Price Stability in the Euro Area. Discussion papers no. 1981, DIW Berlin.

Bevacqua, E., Rakovec, O., Schumacher, D. L., Kumar, R., Thober, S., Samaniego, L., Seneviratne, S. I., and Zscheischler, J. (2024). Direct and lagged climate change effects intensified the 2022 European drought. *Nature Geoscience*, 17:1100—-1107.

Bojinski, S., Verstraete, M. M., Peterson, T. C., Richter, C., Simmons, A., and Zemp, M. (2014). The concept of essential climate variables in support of climate research, applications, and policy. *Bulletin of the American Meteorological Society*, 95(9):1431–1443.

Breiman, L. (2001). Random forests. *Machine Learning*, 45(1):5–32.

Cammalleri, C., Naumann, G., Mentaschi, L., Formetta, G., Forzieri, G., Gosling, S., Bisselink, B., De Roo, A., and Feyen, L. (2020). Global warming and drought impacts in the EU – JRC PESETA IV Project – Task 7. Report EUR 29956 EN, European Commission, Joint Research Centre.

Cammalleri, C., Vogt, J., and Salamon, P. (2017). Development of an operational low-flow index for hydrological drought monitoring over Europe. *Hydrological Sciences Journal*, 62(3):346–358.

Ceglar, A., Jwaideh, M., O'Donnell, E., Danieli, F., Pasqua, C., Hutchinson, J., Cimini, F., Sabuco, J., Alvarez, J., Ranger, N., and Heemskerk, I. (2025). Nature at Risk: Implications for the Euro Area Economy and Financial Stability. Occasional Paper Series 380, European Central Bank.

Chen, T. and Guestrin, C. (2016). Xgboost: A scalable tree boosting system. In *Proceedings of the 22nd ACM SIGKDD International Conference on Knowledge Discovery and Data Mining*, pages 785–794. ACM.

Ciccarelli, M., Kuik, F., and Martínez Hernández, C. (2023). The asymmetric effects of weather shocks on euro area inflation. ECB Working Paper 2798, European Central Bank.

De Roo, A. P. J., Wesseling, C. G., and Van Deursen, W. P. A. (2000). Physically based river basin modelling within a GIS: the LISFLOOD model. *Hydrological Processes*, 14(11-12):1981–1992.

Dell, M., Jones, B. F., and Olken, B. A. (2014). What do we learn from the weather? the new climate-economy literature. *Journal of Economic Literature*, 52(3):740–798.

Dellink, R., Lanzi, E., and Chateau, J. (2019). The sectoral and regional economic consequences of climate change to 2060. *Environmental and Resource Economics*, 72:309–363.

Diebold, F. X. (2012). *Elements of Forecasting*. South-Western Cengage Learning, 4 edition.

Duo, J. (2025). Impact of Climate Policy Uncertainty on Energy Price Volatility: Evidence from China. *Modern Economy*, 16(6):884–903.

European Commission (2021). Commission staff working document: Annual single market report 2021. Commission Staff Working Document SWD(2021) 351 final, European Commission. Accompanying the Communication from the Commission to the European Parliament, the Council, the European Economic and Social Committee and the Committee of the Regions, "Updating the 2020 New Industrial Strategy: Building a stronger Single Market for Europe's recovery".

European Commission Joint Research Centre (2025). Combined Drought Indicators in Europe during winter and spring 2023. Technical Report. Highlights dry conditions affecting agriculture in winter–spring 2023 across Italy, France, Germany, Poland, and the UK.

European Environment Agency (2024). European climate risk assessment. EEA Report 1, Publications Office of the European Union, Luxembourg.

European Environment Agency (2025). Drought impact on ecosystems in Europe. Indicator assessment, European Environment Agency.

European Environment Agency (2026). Building climate-resilient agriculture in europe: an economic perspective. EEA Briefing 03/2026, European Environment Agency. HTML: TH-01-26-009-EN-Q.

Eurostat (2024). Key indicators of physical energy flow accounts by nace rev. 2 activity (env_ac_pefa04). Indicator used: EPRD_ICNS (Intermediate consumption of energy products), EU countries, 2019.

Eurostat (2026). Gross value added and income by main industry (nace rev. 2) – annual data. Dataset code: nama_10_a10__custom_21163016. Last updated: 2026-04-23 23:00. Data extracted: 2026-04-24 14:31:46.

García-León, D., Casanueva, A., Standardi, G., Burgstall, A., Flouris, A. D., and Nybo, L. (2021). Current and projected regional economic impacts of heatwaves in Europe. *Nature Communications*, 12(5807).

Golub, A., Govorukha, K., Mayer, P., and Rübbelke, D. (2022). Climate Change and the Vulnerability of Germany's Power Sector to Heat and Drought. *The Energy Journal*, 43(3):157–184.

Guarascio, D., Reljic, J., and Zezza, F. (2025). Energy vulnerability and resilience in the eu: concepts, empirics and policy. *Journal of Industrial and Business Economics*, 52:683–726.

Guerrieri, V., Lorenzoni, G., Straub, L., and Werning, I. (2022). Macroeconomic implications of covid-19: Can negative supply shocks cause demand shortages? *American Economic Review*, 112(5):1437–1474.

Hao, Z., Singh, V. P., and Xia, Y. (2018). Seasonal drought prediction: Advances, challenges, and future prospects. *Reviews of Geophysics*, 56(1):108–141.

Ionita, M., Caldarescu, D. E., and Nagavciuc, V. (2021). Compound Hot and Dry Events in Europe: Variability and Large-Scale Drivers. *Frontiers in Climate*, 3.

Kahn, M. E., Mohaddes, K., Ng, R. N., Pesaran, M. H., Raissi, M., and Yang, J.-C. (2021). Long-term macroeconomic effects of climate change: A cross-country analysis. *Energy Economics*, 104(105624).

Kotz, M., Donat, M. G., Lancaster, T., Parker, M., Smith, P., Taylor, A., and Vetter, S. H. (2025). Climate extremes, food price spikes, and their wider societal risks. *Environmental Research Letters*, 20(8).

Kuzin, V., Marcellino, M., and Schumacher, C. (2011). MIDAS versus Mixed-Frequency VAR: Nowcasting GDP in the Euro Area. *International Journal of Forecasting*, 27(2):529–542.

Lavaysse, C., Cammalleri, C., Dosio, A., Van Der Schrier, G., Toreti, A., and Vogt, J. (2018). Towards a monitoring system of temperature extremes in Europe. *Natural Hazards and Earth System Sciences*, 18:91–104.

Lesk, C., Anderson, W., Rigden, A., Coast, O., Jägermeyr, J., McDermid, S., Davis, K. F., and Konar, M. (2022). Compound heat and moisture extreme impacts on global crop yields under climate change. *Nature Reviews Earth & Environment*, 3:872–889.

Li, Z., Long, J., and Li, L. (2024). A novel machine learning ensemble forecasting model based on mixed frequency technology and multi-objective optimization for carbon trading price. *Frontiers Energy Resources*, 11.

Lundberg, S., Erion, G. G., and Lee, S.-I. (2018). Consistent individualized feature attribution for tree ensembles. *arXiv*.

Martín Cervantes, P. A., Rueda López, N., and Cruz Rambaud, S. (2020). The effect of globalization on economic development indicators: An inter-regional approach. *Sustainability*, 12(5):19–42.

Mátyás, L., editor (2022). *Emerging European Economies after the Pandemic: Stuck in the Middle Income Trap?* Contributions to Economics. Springer, Cham.

McKee, T. B., Doesken, N. J., and Kleist, J. (1993). The relationship of drought frequency and duration to time scale. In *Proceedings of the Eighth Conference on Applied Climatology*, Anaheim, California. American Meteorological Society.

Mohaddes, K., Ng, R. N., Pesaran, M. H., Raissi, M., and Yang, J.-C. (2023). Climate change and economic activity: evidence from US states. *Oxford Open Economics*, 2.

Nichifor, B., Zait, L., and Turcu, O. (2025). Renewable investments, environmental spending, and emissions in eastern europe: A spatial-economic analysis of management and policy decisions efficiency. *Sustainability*, 17(7):3010.

Pargent, F., Pfisterer, F., Thomas, J., and Bischl, B. (2022). Regularized target encoding outperforms traditional methods in supervised machine learning with high cardinality features. *Computational Statistics*, 37:2671–2692.

Parker, M. (2016). Global inflation: the role of food, housing and energy prices. Discussion paper no. 2016/05, Reserve Bank of New Zealand.

Peersman, G. (2022). International Food Commodity Prices and Missing (Dis)Inflation in the Euro Area. *The Review of Economics and Statistics*, 104(1):85–100.

Pinke, Z., Ács, T., Kalicz, P., Kern, Z., and Jambor, A. (2024). Hotspots in the EU-27 and Economic Consequences of the 2022 Spring–Summer Drought. *EuroChoices*, 23(1):28–33.

Prokhorenkova, L., Gusev, G., Vorobev, A., Dorogush, A. V., and Gulin, A. (2018). CatBoost: Unbiased boosting with categorical features. In *NIPS'18: Proceedings of the 32nd International Conference on Neural Information Processing Systems*, pages 6639–6649.

Publications Office of the European Union (2026). Eurovoc: Geographical classification. https://op.europa.eu/en/web/eu-vocabularies/concept-scheme/-/resource?uri=http://eurovoc.europa.eu/100277. Accessed: 2026-04-23.

Rossi, L., Wens, M., De Moel, H., Cotti, D., Sabino Siemons, A., Toreti, A., Maetens, W., Masante, D., Van Loon, A., Hagenlocher, M., Rudari, R., Naumann, G., Meroni, M., Avanzi, F., Isabellon, M., and Barbosa, P. (2023). European drought risk atlas. Technical Report JRC135215, European Commission, Joint Research Centre, Publications Office of the European Union, Luxembourg.

Russo, S., Sillmann, J., and Fischer, E. M. (2015). Top ten European heatwaves since 1950 and their occurrence in the coming decades. *Environmental Research Letters*, 10(124003).

Santa, R., Bošnjaković, M., Rajcsanyi-Molnar, M., and Andras, I. (2025). Energy systems in transition: A regional analysis of eastern europe's energy challenges. *Clean Technologies*, 7(4):84.

Seneviratne, S. I., Zhang, X., Adnan, M., Badi, W., Dereczynski, C., Luca, A. D., Ghosh, S., Iskandar, I., Kossin, J., Lewis, S., Otto, F., Pinto, I., Satoh, M., Vicente-Serrano, S. M., Wehner, M., and Zhou, B. (2021). Climate change 2021: The physical science basis. weather and climate extreme events in a changing climate. Technical report, Intergovernmental Panel on Climate

Change. Contribution of Working Group I to the Sixth Assessment Report of the Intergovernmental Panel on Climate Change.

Sepulcre-Canto, G., Horion, S., Singleton, A., Carrao, H., and Vogt, J. (2012). Development of a Combined Drought Indicator to detect agricultural drought in Europe. *Natural Hazards and Earth System Sciences*, 12(11):3519–3531.

Shapley, L. S. (1953). A Value for N-Person Games. *Contributions to the Theory of Games*, 2:307–317.

Sun, Y., Zhu, S., Wang, D., Duan, J., Lu, H., Yin, H., Tan, C., Zhang, L., Zhao, M., Cai, W., Wang, Y., Hu, Y., Tao, S., and Guan, D. (2024). Global supply chains amplify economic costs of future extreme heat risk. *Nature*, 627:797–804.

Tabari, H. and Willems, P. (2023). Global risk assessment of compound hot-dry events in the context of future climate change and socioeconomic factors. *npj Climate and Atmospheric Science*, 6(74).

Toreti, A., Bavera, D., Acosta Navarro, J., Acquafresca, L., Azas, K., Barbosa, P., de Jager, A., Ficchi, A., Fioravanti, G., Grimaldi, S., Hrast Essenfelder, A., Magni, D., Mazzeschi, M., McCormick, N., Salamon, P., Santos Nunes, S., and Volpi, D. (2024). Drought in Europe – July 2024. GDO Analytical Report JRC138930, European Commission, Joint Research Centre, Luxembourg: Publications Office of the European Union.

Toreti, A., Bavera, D., Cammalleri, C., Cota, T., De Jager, A., Deus, R., Di Ciollo, C., Maetens, W., Magni, D., Masante, D., Mazzeschi, M., Mccormick, N., Cabrinha Pires, V., Quadrado, M. F., Saramago, M. M., and Spinoni, J. (2022). Drought in western Mediterranean February 2022. GDO Analytical Report JRC128743, European Commission, Joint Research Centre, Luxembourg: Publications Office of the European Union.

Toreti, A., Belward, A., Perez-Dominguez, I., Naumann, G., Luterbacher, J., Cronie, O., Seguini, L., Manfron, G., Lopez Lozano, R., Baruth, B., Van Den Berg, M., Dentener, F., Ceglar, A., Chatzopoulos, T., and Zampieri, M. (2019). The exceptional 2018 European water seesaw calls for action on adaptation. *Earth's Future*, 7(6):652–663. JRC114198.

Tripathy, K. P. and Mishra, A. K. (2023). How unusual is the 2022 european compound drought and heatwave event? *Geophysical Research Letters*, 50(15):e2023GL105453.

Usman, S., González-Torres Fernández, G., and Parker, M. (2025a). Going nuts: The regional impact of extreme climate events over the medium term. *European Economic Review*, 178:105081.

Usman, S., Parker, M., and Vallat, M. (2025b). Dry-roasted NUTS: Early Estimates of the Regional Impact of 2025 Extreme Weather. *SSRN*.

Vanschoenwinkel, J., Mendelsohn, R., and Van Passel, S. (2016). Do western and eastern europe have the same agricultural climate response? taking adaptive capacity into account. *Global Environmental Change*, 41:74–87.

Wegner, O., Dees, S., Boullot, M., Lesterquy, P., Serfaty, C., Thubin, C., Ulgazi, Y., Boitout, A., and Gabet, M. (2025). Seeds of Inflation: Macro Modelling of Nature-Related Risks through Agricultural Prices. Working Paper Series 1006, Banque de France, Paris, France.

Wooldridge, J. M. (2010). *Econometric Analysis of Cross Section and Panel Data*. MIT Press, Cambridge, MA, 2 edition.

Yin, J. and Slater, L. (2023). Understanding heatwave-drought compound hazards and impacts on socio-ecosystems. *The Innovation Geoscience*, 1(3). 100042.

Zajac, Z., Gomez, O., Gelati, E., van der Velde, M., Bassu, S., Ceglar, A., Chukaliev, O., Panarello, L., Koeble, R., van den Berg, M., Niemeyer, S., and Fumagalli, D. (2022). Estimation of spatial distribution of irrigated crop areas in europe for large-scale modelling applications. *Agricultural Water Management*, 266:107527.

Zhang, X. and Tong, H. (2022). Asymptotic theory of principal component analysis for time series data with cautionary comments. *Journal of the Royal Statistical Society Series A - Statistics in Society)*, 185(2):543–565.

Zhu, W. and Li, S. (2024). Nonlinear effects of climate risks on climate-sensitive sectors. *Economic Change and Restructuring*, 57(167).

Zscheischler, J. and Fischer, E. M. (2020). The record-breaking compound hot and dry 2018 growing season in Germany. *Weather and Climate Extremes*, 29(100270).

Appendix

Figure A.1: Total Nominal GVA per capita

(a) Nominal GVA per capita in 2005 **(b)** Annualised growth rate between 2005 & 2022

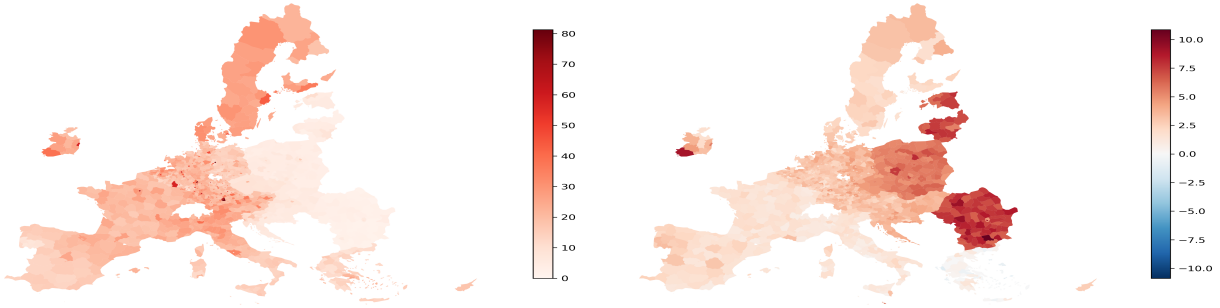

Note: Figure A.1 illustrates the economic growth patterns across Europe. Panel (a) presents the total GVA per capita in 2005, using a gradient to represent regional differences. Panel (b) shows the annualised growth rate over the period 2005–2022, calculated as the average annual percentage change in GVA per capita. The year 2005 is used as the starting point because data for some regions were unavailable in earlier years.
Source: Eurostat and authors' calculations.

Figure A.2: Heat Waves over the Hotter Months (May to September)

(a) Average Heat Wave Days in 2002-2006 **(b)** Change in Averages between 2018-2022 & 2002-2006

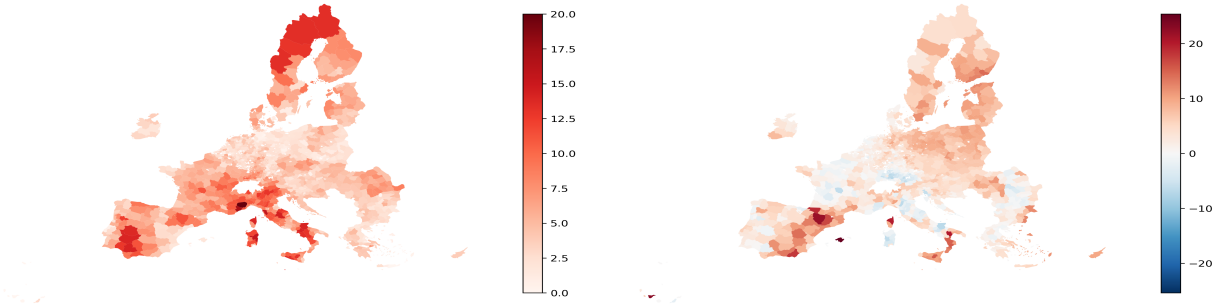

Note: Figure A.2 illustrates heat wave patterns across Europe during the summer months (May to September). Panel (a) presents the average annual number of heat wave days recorded between 2002 and 2006, using a white-to-dark red gradient (0 to 20 average heat wave days). Panel (b) depicts the change in frequency between 2018 and 2022 relative to the earlier period, calculated as the average annual number of heat wave days in 2018–2022 minus that of 2002–2006. The colour gradients convey the intensity of heat wave activity, with red indicating an increase in frequency and blue representing a decline.
Source: Authors' calculations using HCWI from the Copernicus European Drought Observatory.

Figure A.3: Average Number of Heat Wave Months (Mean HCWI > 0) per Year

(a) Average Number of Months in 2002-2006 **(b)** Change in Averages between 2018-2022 & 2002-2006

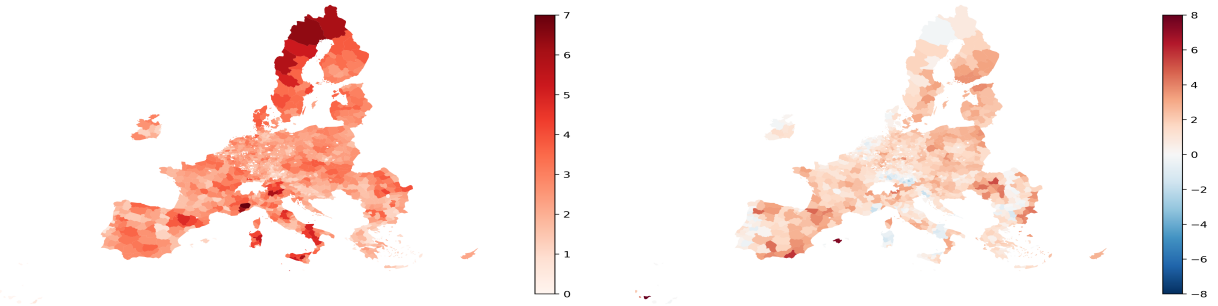

Note: Figure A.3 compares heat wave month patterns across Europe. Panel (a) presents the average number of heat wave months recorded between 2002 and 2006, using a white-to-dark red gradient (0 to 7 months). Panel (b) depicts the change in averages between 2018–2022 and 2002–2006, with a blue-to-red gradient indicating decreases and increases, respectively. Heat wave months are defined as those with mean HCWI values above 0.
Source: Authors' calculations using HCWI from the Copernicus European Drought Observatory.

Figure A.4: Average Number of Meteorological Dry Months (Mean SPI01 ≤ -1) per Year

(a) Average Number of Months in 2002-2006 **(b)** Change in Averages between 2018-2022 & 2002-2006

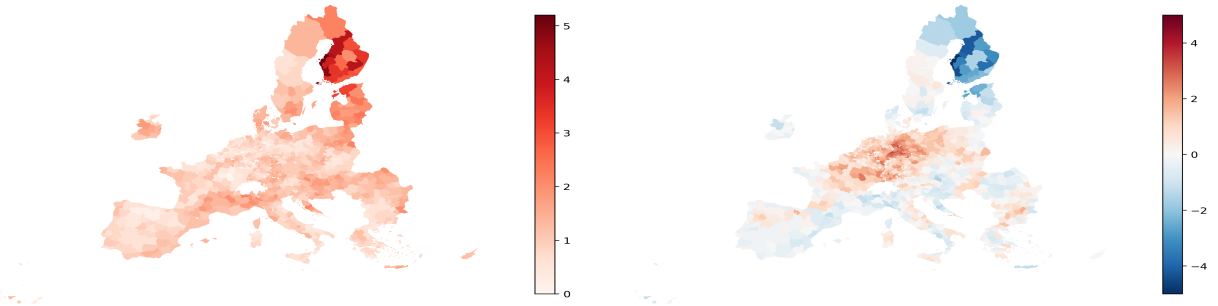

Note: Figure A.4 compares meteorological dry month patterns across Europe. Panel (a) shows the average number of dry months per year from 2002–2006, using a white-to-dark red gradient (0 to 5 months). Panel (b) displays the change in averages between 2018–2022 and 2002–2006, with a blue-to-red gradient indicating decreases and increases, respectively. Dry months are defined as those with mean SPI01 values below −1.
Source: Authors' calculations using SPI01 from the Copernicus European Drought Observatory.

Figure A.5: Average Number of Hydrological Dry Months (Mean LFI > 0) per Year

(a) Average Number of Months in 2002-2006 **(b)** Change in Averages between 2018-2022 & 2002-2006

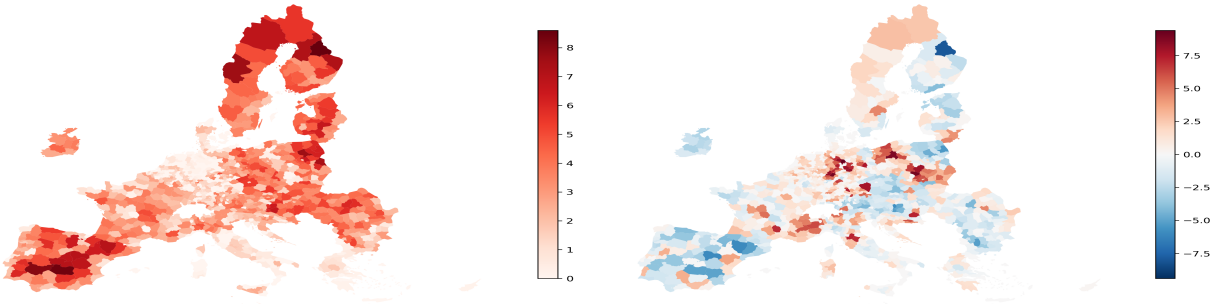

Note: Figure A.5 compares hydrological dry month patterns across Europe at the NUTS-3 regional level. Panel (a) shows the average number of dry months per year from 2002–2006, using a white-to-dark red gradient (0 to 8 months). Panel (b) displays the change in averages between 2018–2022 and 2002–2006, with a blue-to-red gradient indicating decreases and increases, respectively. Dry months are defined as those with mean LFI values above 0.
Source: Authors' calculations using LFI from the Copernicus European Drought Observatory.

Figure A.6: Average Number of Agricultural Dry Months (Mean SMA ≤ -1) per Year

(a) Average Number of Months in 2002-2006 **(b)** Change in Averages between 2018-2022 & 2002-2006

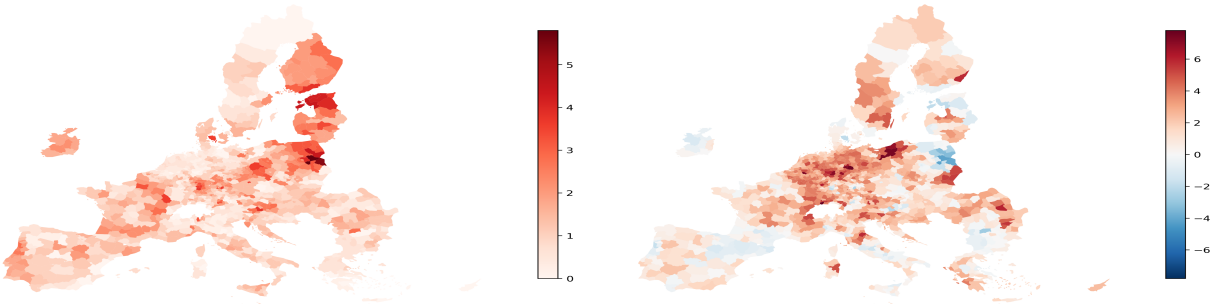

Note: Figure A.6 compares agricultural dry month patterns across Europe at the NUTS-3 regional level. Panel (a) shows the average number of dry months per year from 2002–2006, using a white-to-dark red gradient (0 to 5 months). Panel (b) displays the change in averages between 2018–2022 and 2002–2006, with a blue-to-red gradient indicating decreases and increases, respectively. Dry months are defined as those with mean SMA values below −1.
Source: Authors' calculations using SMA from the Copernicus European Drought Observatory.

Figure A.7: Average Number of Agricultural Dry Months (Mean fAPAR $\leq$ -1) per Year

(a) Average Number of Months in 2003-2012 **(b)** Change in Averages between 2013-2022 & 2003-2012

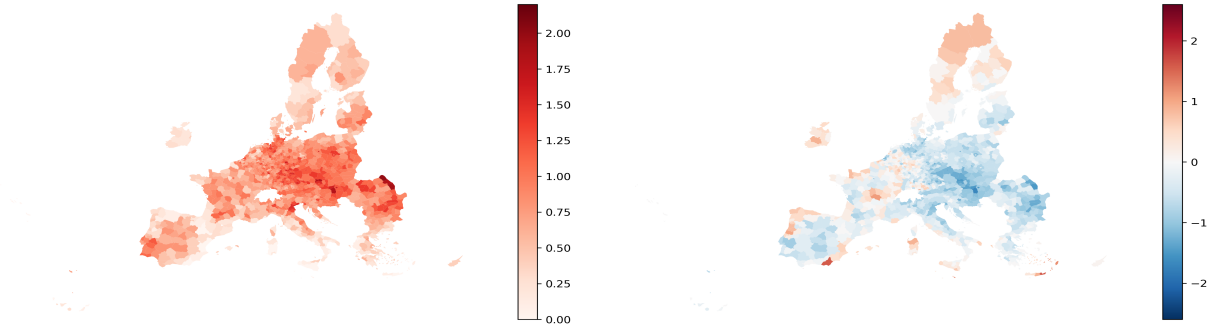

Note: Figure A.7 compares agricultural dry month patterns across Europe. Panel (a) shows the average number of dry months per year from 2003–2012, using a white-to-dark red gradient (0 to 2 months). Panel (b) displays the change in averages between 2013–2022 and 2003–2012, with a blue-to-red gradient indicating decreases and increases, respectively. Dry months are defined as those with mean fAPAR values below −1. A 10-year horizon is chosen here, rather than a 5-year horizon as with the other variables, to smooth out inter-annual variability in fAPAR and better capture long-term trends in agricultural drought patterns.
Source: Authors' calculations using fAPAR from the Copernicus European Drought Observatory.

Figure A.8: Deviation of Yearly Simulated Outcomes with 2022 Percentiles from Sample Extremes

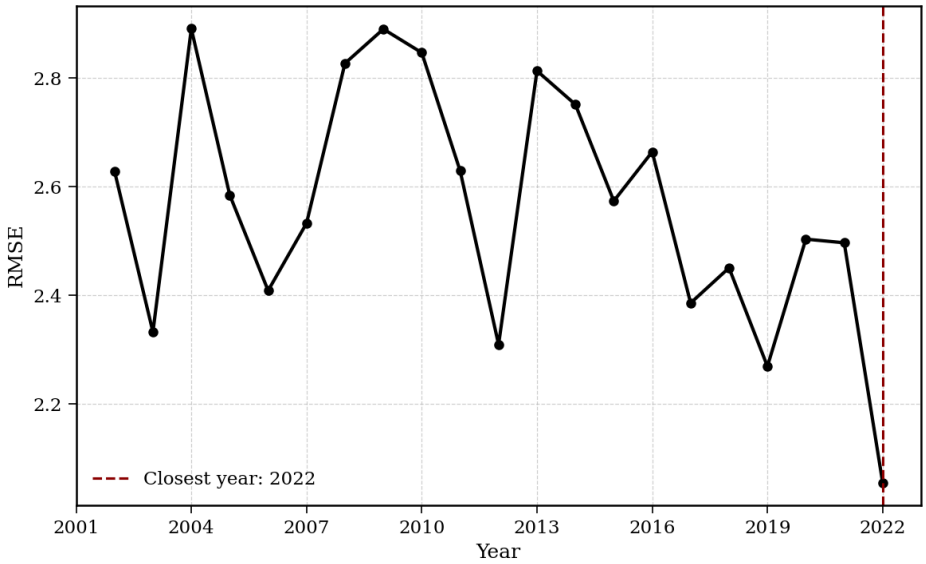

Note: The figure displays the RMSE between the simulated outcomes when using the simulation datasets D^{γ^*} and D^{**}, as defined in Equation 8 and Equation 9 of Section 5.1. D^{γ^*} and D^{**} highlight 2022 only and the entire dataset based climate extremes, respectively.
Source: Authors' calculations

Figure A.9: Intermediate Consumption of Energy Products

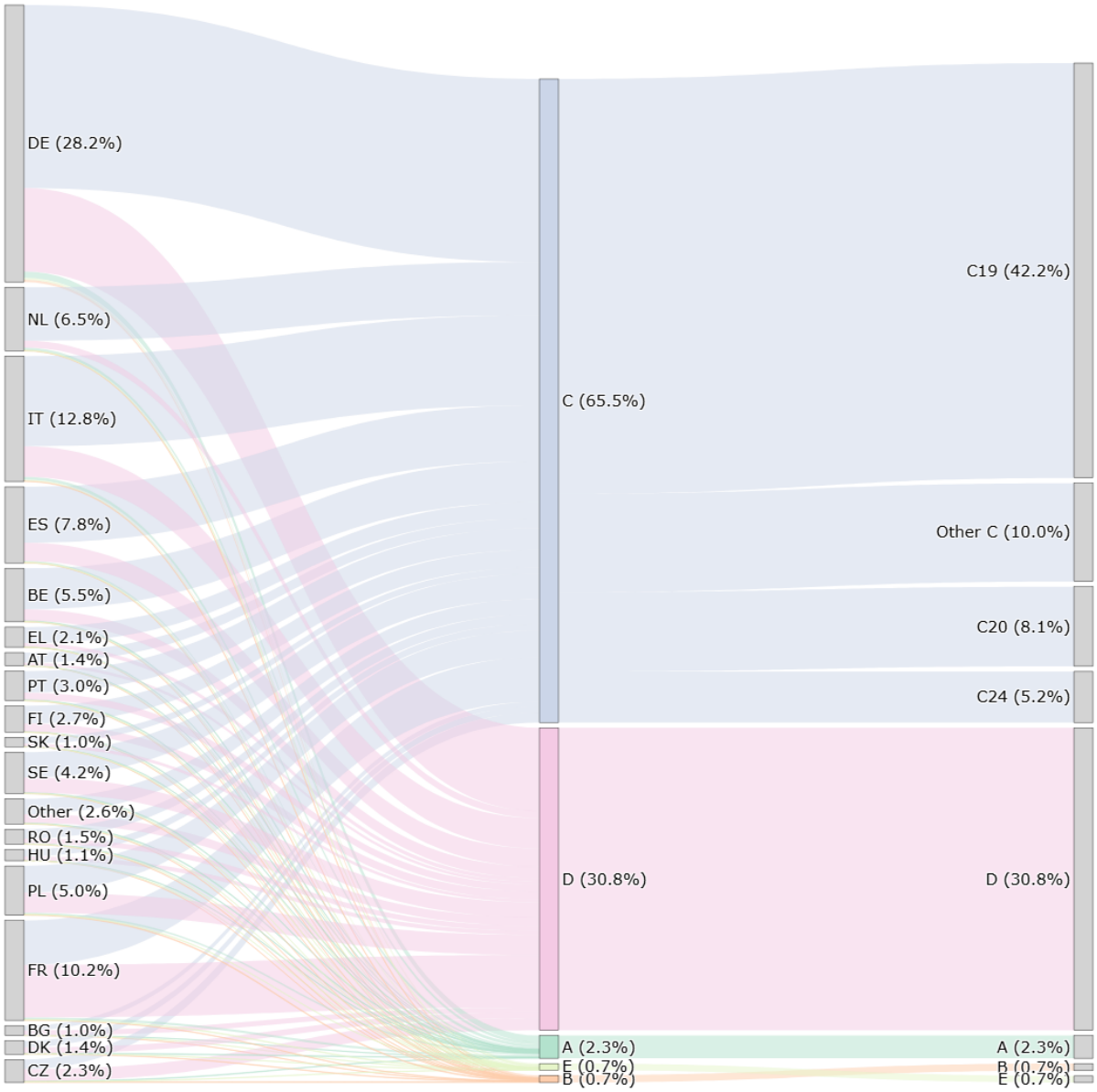

Note: The figure illustrates the intermediate consumption of energy products (PEFA, EPRD ICNS) across sectors A, B, C, D and E between 2002 and 2022.
Source: Authors' calculations using Eurostat (2024) data.

Figure A.10: Robust Simulation of Heat Waves and Droughts on Sector A

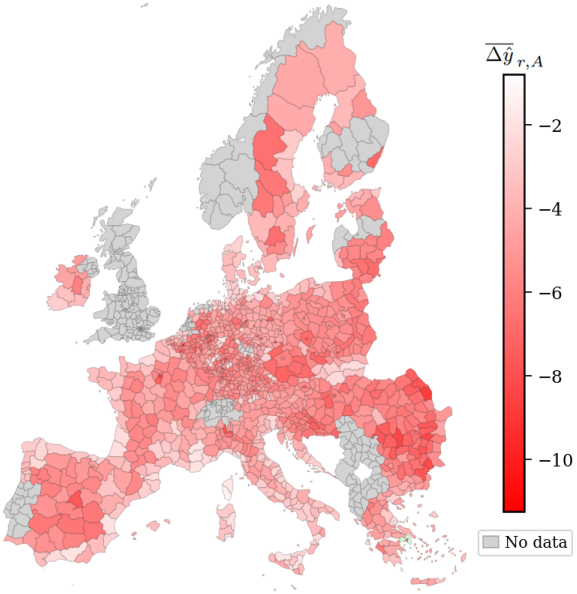

Note: The Figure illustrates $\overline{\Delta\hat{y}_{r,s}}$ on agricultural (A) real per capita GVA growth under a compound heat wave and drought, computed as the $1^{st}/99^{th}$ percentile of climate variables over the 2002-2022 periods across all EU regions, evaluated under the averaged economic conditions of the period. Values are mapped from green to red, indicating positive to negative differences of up to ten percentage points. Simulated outcomes are unavailable for regions in Germany, Finland, Latvia, the Netherlands, and Portugal (shown in grey) because the underlying economic data were unavailable at the time of collection.
Source: Authors' calculations

Figure A.11: Robust Simulation of Heat Waves and Droughts on Sectoral Aggregates B-E (left) & C (right)

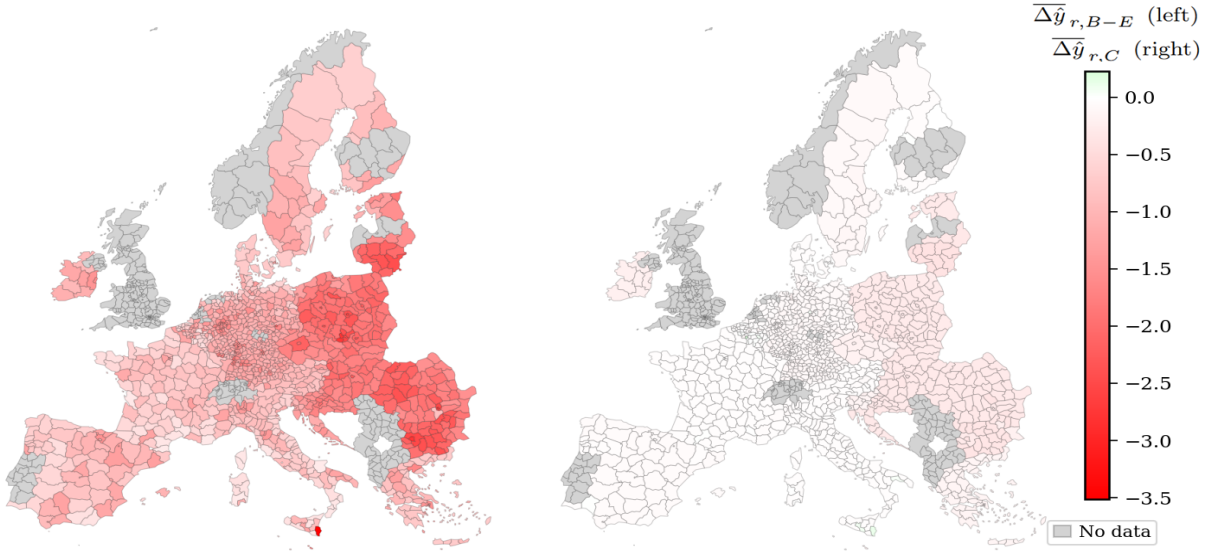

Note: The Figure illustrates $\overline{\Delta\hat{y}_{r,s}}$ on industrial (B-E, left) and manufacturing (C, right) real per capita GVA growth under a compound heat wave and drought, computed as the $1^{st}/99^{th}$ percentile of climate variables over the 2002-2022 periods across all EU regions. Values are mapped from green to red, indicating positive to negative differences of up to four percentage points. Simulated outcomes are unavailable for regions in Germany, Finland, Latvia, the Netherlands, and Portugal (shown in grey) because the underlying economic data were unavailable at the time of collection.
Source: Authors' calculations

Figure A.12: Yearly Dispersion of $\Delta\hat{y}_{t,r,A}$, $\Delta\hat{y}_{t,r,B-E}$ and $\Delta\hat{y}_{t,r,C}$.

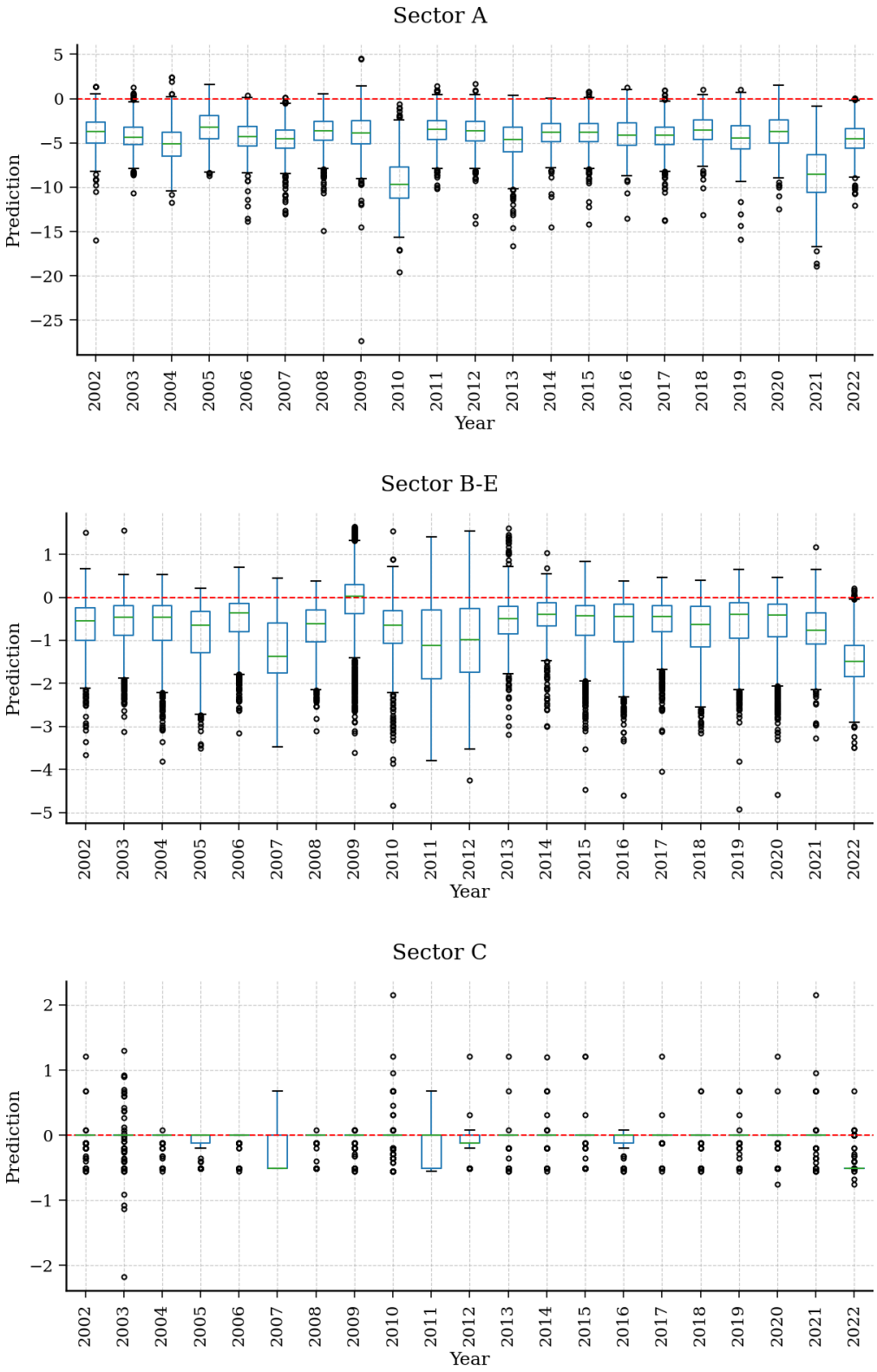

Note: The figure presents the yearly dispersion of the estimated prediction differentials, between the event and non-event scenarios, across sectors A, B–E, and C over the period 2002–2022 using boxplots.
Source: Authors' calculations

Table A.1: Average SPI and HCWI Values by Country and Period

	Average Values Over 2002–2006				Average Values Over 2018–2022			
Country	**SPI01**	**SPI06**	**SPI12**	**HCWI**	**SPI01**	**SPI06**	**SPI12**	**HCWI**
Austria	0.0000	-0.0058	-0.0084	0.6131	0.0000	-0.0268	-0.0558	1.2414
Belgium	0.0000	-0.0125	-0.0438	0.7507	-0.0180	-0.2210	-0.2585	0.9366
Bulgaria	0.0000	0.0000	0.0000	0.5963	-0.0146	0.0000	-0.0147	0.8442
Cyprus	0.0000	0.0000	-0.2091	0.6297	0.000	0.0000	0.0000	1.5645
Czech Republic	0.0000	0.0000	0.0000	0.9195	0.0000	-0.0167	-0.0383	1.5161
Germany	0.0000	-0.0044	-0.0329	0.6947	-0.0136	-0.1796	-0.2810	0.9897
Denmark	0.0000	0.0000	-0.0478	0.7650	0.0000	0.0000	-0.0202	1.2358
Estonia	0.0000	-0.4699	-0.4995	1.0835	0.0000	0.0000	0.0000	1.9151
Greece	0.0000	0.0000	0.0000	0.3528	-0.0069	-0.0418	-0.0488	0.8192
Spain	0.0000	-0.0888	-0.1499	0.6050	0.0000	-0.0045	-0.0153	1.4302
Finland	-0.1511	-0.6627	-0.8369	1.1448	0.0000	0.0000	-0.0119	1.7958
France	0.0000	-0.0257	-0.0638	0.8064	-0.0199	-0.0300	-0.0342	1.3075
Croatia	0.0000	0.0000	0.0000	0.5485	0.0000	0.0000	0.0000	0.8604
Hungary	0.0000	-0.0224	-0.0749	0.6807	0.0000	-0.0552	-0.0913	1.1856
Ireland	0.0000	0.0000	0.0000	0.4099	0.0000	0.0000	0.0000	0.6715
Italy	0.0000	-0.0079	-0.0823	1.0521	-0.0205	-0.0783	-0.0795	1.4173
Lithuania	0.0000	-0.1965	-0.2204	0.8041	-0.0430	0.0000	-0.1123	1.6761
Luxembourg	0.0000	0.0000	-0.4149	0.9569	0.0000	0.0000	0.0000	1.4145
Latvia	0.0000	-0.2935	-0.2907	1.0554	0.0000	-0.0471	-0.2489	1.9054
Malta	0.0000	-0.2156	-0.3345	0.4721	0.0000	0.0000	0.0000	0.8198
Netherlands	0.0000	0.0000	0.0000	0.6678	-0.0069	-0.0326	-0.1974	0.7780
Poland	0.0000	0.0000	-0.0091	0.7130	-0.0948	-0.0103	-0.0170	1.3940
Portugal	0.0000	-0.1631	-0.2619	0.5536	-0.0449	-0.0376	-0.1162	0.7040
Romania	0.0000	0.0000	0.0000	0.6957	-0.0055	0.0000	0.0000	1.3178
Sweden	0.0000	-0.0100	-0.0228	1.0263	-0.0417	0.0000	0.0000	1.6997
Slovenia	0.0000	0.0000	0.0000	0.5543	0.0000	0.0000	0.0000	0.8222
Slovakia	0.0000	0.0000	0.0000	0.7944	0.0000	0.0000	0.0000	1.4916

Note: Table A.1 displays the average values of SPI across the accumulation periods of 1, 6 and 12 months, and HCWI during the five year periods of 2002 to 2006 and 2018 to 2022. Dryer (Hotter) conditions over time are suggested by smaller (larger) values in the 2018-2022 period, relative to that of 2002-2006.
Source: Authors' calculations using SPI and HCWI from the Copernicus European Drought Observatory.

Table A.2: Predictions' RMSEs by Year

Model	Linear Regression			Random Forest			XGBoost		
	A	B–E	C	A	B–E	C	A	B–E	C
Economic (f_{ECON})									
– 2018	21.31	15.34	15.36	19.88	15.20	15.38	42.04	15.27	15.17
– 2019	18.78	8.66	8.29	22.14	8.48	9.07	25.60	8.64	7.94
– 2020	18.67	12.20	12.85	21.42	12.05	14.52	19.81	11.83	12.34
– 2021	19.40	17.02	171.79	22.67	16.81	160.55	19.56	16.72	169.68
– 2022	28.45	15.72	19.08	28.24	15.01	14.08	27.64	15.40	14.30
Climate (f_{CLIM})									
- Medians & St. Deviations									
– 2018	20.06	15.40	15.37	16.36	15.26	15.20	16.27	15.29	15.20
– 2019	18.39	8.62	8.22	19.01	8.54	8.37	18.79	8.69	7.95
– 2020	18.11	12.25	12.83	17.97	12.19	13.86	17.86	12.21	12.44
– 2021	19.75	17.17	171.88	19.71	17.09	162.53	19.29	16.81	171.85
– 2022	31.41	15.89	19.15	29.15	15.31	14.23	28.28	15.25	14.18
- PCA Features									
– 2018	23.20	15.36	15.37	15.72	15.23	15.27	21.23	15.27	16.85
– 2019	17.76	8.78	8.37	20.20	8.61	8.61	19.00	8.60	9.40
– 2020	17.66	12.07	12.66	17.95	11.99	14.17	17.64	12.18	12.57
– 2021	19.06	17.03	171.79	19.50	17.05	163.38	19.36	17.19	171.81
– 2022	30.69	15.97	19.26	29.28	15.22	14.17	28.57	15.26	14.49
- MIDAS Features									
– 2018	21.43	15.42	15.42	14.45	15.26	15.37	16.77	15.28	15.28
– 2019	19.43	8.94	8.53	19.74	8.54	8.73	17.74	12.04	12.47
– 2020	18.11	12.64	13.15	18.29	12.21	14.11	17.74	12.04	12.47
– 2021	19.25	17.35	172.02	19.57	17.32	165.96	19.26	16.99	187.67
– 2022	33.22	15.90	19.15	30.45	15.29	14.66	29.34	15.35	23.02

Note: The reported RMSEs represents the aggregate out-of-sample prediction error, evaluated across all horizons using recursively generated expanding-window predictions and observed outcomes. RMSEs are calculated over annual one-step ahead predictions of real growth in per capita GVA for every year in the evaluation period. Sector A covers agriculture; B–E includes mining (B), manufacturing (C), utilities (D), and waste management (E), with C also modelled separately to obtain direct predictions for manufacturing.

Table A.3: Pre-Pandemic Predictions' RMSEs

Model	Linear Regression			Random Forest			XGBoost		
	A	B–E	C	A	B–E	C	A	B–E	C
Economic (f_{ECON})	20.08	12.46	12.34	21.04	$12.31^{\dagger}$	12.63	34.81	$12.41^{\dagger}$	$12.11^{\dagger}$
Climate (f_{CLIM})									
- Medians & St. Deviations	19.25^{*}	12.48	12.32	$17.74^{*\dagger}\S$	$12.37^{\dagger}\S$	12.27^{*}	$17.58^{*\dagger}\S$	12.44	12.13
- PCA Features	20.66	12.51	12.37	$18.10^{*\dagger}\S$	$12.37^{\dagger}\S$	12.39^{*}	$20.15^{*\dagger}$	12.39	13.64
- MIDAS Features	20.45	12.60	12.46	$17.30^{*\dagger}\S$	$12.36^{\dagger}\S$	12.50^{*}	$20.15^{*\dagger}$	$12.37^{\dagger}$	15.90

Note: The reported RMSEs represents the aggregate out-of-sample prediction error, using recursively generated expanding-window predictions and observed outcomes. RMSEs are calculated over annual predictions of real growth in per capita GVA from 2018 to 2019. Sector A covers agriculture; B–E includes mining (B), manufacturing (C), utilities (D), and waste management (E), with C also modelled separately to obtain direct predictions for manufacturing. Symbols denote statistically significant improvements in predictive performance as:
* $p < 0.05$ indicates predictive improvements relative to the respective economic counterpart of the same model type;
† $p < 0.05$ indicates predictive improvements relative to the respective linear regression counterpart; and
§ $p < 0.05$ indicates predictive improvements relative to the respective linear economic model for the same sector.

Table A.4: Distribution of Features' SHAP Values of Economic Random Forest Models

	Mean	St.Dev.	Min.	25%	50%	75%	Max.
			Sector A				
$Y_{t-1,r,s}$	-0.2454	4.5496	-15.0804	-2.9498	-1.0047	1.0390	38.4100
$G_{t-1,c}$	0.9561	3.5584	-18.0345	-1.5119	0.6861	3.4000	20.5366
N_r	-0.3810	1.5682	-7.2457	-1.4716	0.1484	0.6369	13.6649
$E_{t,r,s}$	0.2378	9.2843	-3.9785	-0.6121	-0.2259	0.1830	32.6453
M_r	0.0407	0.3971	-2.2521	-0.0668	0.0932	0.1875	1.5114
C_r	0.0021	0.3204	-2.6496	-0.1214	0.1125	0.1839	0.9988
U_r	0.0112	0.1518	-2.2309	-0.0284	-0.0051	0.0141	3.6841
R_r	0.0104	0.0703	-0.5019	-0.0239	-0.0035	0.0312	0.4177
			Sector B-E				
$G_{t-1,c}$	0.6982	1.4535	-2.3878	-0.5821	0.2494	1.7418	7.0956
$E_{t,r,s}$	-0.0214	0.6931	-6.9040	-0.4270	0.1964	0.3911	2.8364
$Y_{t-1,r,s}$	-0.0325	1.1390	-5.5865	-0.2547	-0.1901	-0.1119	16.2900
C_r	0.0067	0.4615	-5.1442	-0.2267	0.1845	0.2461	1.8337
U_r	0.0089	0.3101	-5.1565	0.0644	0.1082	0.1452	1.0384
N_r	-0.0668	0.2793	-3.7383	-0.1563	-0.1039	0.0052	4.3249
M_r	-0.0024	0.1884	-1.3772	-0.0363	0.0473	0.0898	0.7549
R_r	-0.0027	0.1366	-0.6759	-0.1002	-0.0569	0.1174	0.6419
			Sector C				
$G_{t-1,c}$	0.9725	2.2731	-6.6462	-0.3940	0.6765	2.2400	39.1430
$Y_{t-1,r,s}$	-0.0364	5.2811	-4.3043	-0.6366	-0.3585	-0.0653	49.5877
C_r	-0.0256	1.0989	-21.1001	-0.2293	0.3169	0.5171	3.4493
$E_{t,r,s}$	0.0990	1.1152	-5.6274	-0.3200	0.1734	0.4867	15.8327
N_r	-0.1763	1.4562	-1.6900	-0.5108	-0.2501	0.0165	49.6542
U_r	0.0341	0.5151	-2.9356	0.0025	0.1270	0.2110	17.3866
M_r	0.0100	0.3916	-9.1788	-0.0945	0.0706	0.2195	5.3141
R_r	-0.0072	0.3170	-1.5420	-0.2083	-0.0537	0.1642	1.5904

Note: The table displays the descriptive statistics of the distribution of SHAP values of the Random Forest economic models. The variables are ordered by feature importance, where the variable with the largest predictive contributions listed first. Beeswarm and dependence plots are made available on request.
Source: Authors' calculations.

Table A.5: Distribution of Features' SHAP Values of Economic XGBoost Models

	Mean	St.Dev.	Min.	25%	50%	75%	Max.
			Sector A				
$Y_{t-1,r,s}$	0.0723	2.6879	-4.9938	-1.3987	-0.5907	0.8541	27.5306
$G_{t-1,c}$	0.1762	1.6866	-2.8521	-1.1275	-0.1886	1.8884	7.1962
N_r	0.0012	0.8669	-1.8084	-0.9873	0.6464	0.7326	2.6126
$E_{t,r,s}$	0.9008	34.6807	-3.0826	-0.1158	-0.0700	-0.0312	15.9659
C_r	0.0073	0.0920	-0.3185	-0.0751	0.0477	0.0768	0.1535
M_r	-0.0097	0.1345	-0.7211	-0.0917	0.0237	0.0273	0.2390
U_r	0.0012	0.0570	-0.1853	-0.0103	-0.0053	0.0028	0.6321
R_r	0.0000	0.0005	-0.0011	-0.0002	-0.0001	0.0002	0.0021
			Sector B-E				
$G_{t-1,c}$	-0.0290	0.7785	-1.7838	-0.5817	-0.1723	0.2237	3.2067
$E_{t,r,s}$	-0.0104	0.2801	-3.4613	-0.2551	0.0880	0.1786	6.0217
$Y_{t-1,r,s}$	0.0149	0.4682	-1.7662	-0.0888	-0.0565	-0.0124	9.9381
C_r	-0.0184	0.1680	-1.4065	-0.1576	0.0625	0.0876	0.4751
N_r	0.0140	0.1841	-1.2827	-0.0783	-0.0342	0.0246	3.8945
U_r	0.0088	0.1309	-0.8732	0.0445	0.0542	0.0625	0.4889
R_r	0.0023	0.0550	-0.6256	-0.0310	-0.0187	0.0489	0.6139
M_r	-0.0044	0.0468	-0.4800	-0.0236	0.0154	0.0232	0.1769
			Sector C				
$G_{t-1,c}$	-0.0807	0.7964	-1.8728	-0.6988	-0.1915	0.5981	7.7891
C_r	-0.0034	0.2994	-13.0342	-0.2849	0.1252	0.1284	0.7585
$E_{t,r,s}$	0.0086	0.2543	-4.7443	-0.1533	0.1179	0.1334	2.7816
$Y_{t-1,r,s}$	0.0339	1.7328	-0.1229	-0.0669	-0.0611	-0.0541	8.2140
N_r	-0.0044	0.3819	-27.3650	-0.0097	-0.0031	0.0053	2.0872
U_r	0.0057	0.0499	-0.3590	0.0039	0.0055	0.0089	1.4593
M_r	-0.0006	0.0059	-0.0259	-0.0049	0.0018	0.0019	0.0178
R_r	-0.0003	0.0052	-0.0429	-0.0031	-0.0017	0.0030	0.0165

Note: The table displays the descriptive statistics of the distribution of SHAP values of the XGBoost economic models. The variables are ordered by feature importance, where the variable with the largest predictive contributions listed first. Beeswarm and dependence plots are made available on request.
Source: Authors' calculations.

Table A.6: Distribution of Features' SHAP Values of Yearly Aggregations Climate Augmented Random Forest Models

	Mean	St.Dev.	Min.	25%	50%	75%	Max.
			Sector A				
$Y_{t-1,r,s}$	-0.0912	3.8483	-13.9467	-2.2517	-0.9210	0.8095	46.2604
$G_{t-1,c}$	0.7632	2.3753	-10.7212	-0.9042	0.8525	2.4364	14.2245
$GC_{t,r}^{\bar{H}CWI}$	-1.1646	2.5712	-16.1377	-3.4810	0.2462	0.7384	5.3786
N_r	-0.1514	1.1189	-6.0591	-0.9220	0.1137	0.5681	18.6694
$\sigma_{t,r}^{GC^{HCWI}}$	-0.2799	0.6047	-3.6598	-0.5842	-0.3069	-0.0422	6.1563
$H\bar{C}WI_{t,r}$	-0.1758	1.2145	-6.1643	-0.5724	0.0306	0.1975	7.6638
$\sigma_{t,r}^{GC^{LFI}}$	-0.0736	0.6858	-3.5606	-0.2326	0.0827	0.2371	4.2825
$E_{t,r,s}$	0.1124	4.6682	-2.7547	-0.3576	-0.1607	0.0479	46.6676
M_r	-0.0345	0.3191	-1.8692	-0.2212	0.0137	0.1146	2.2108
C_r	-0.0150	0.2596	-2.5090	-0.1272	0.0534	0.1512	0.8798
			Sector B-E				
$G_{t-1,c}$	0.4978	1.3364	-2.2372	-0.6292	0.1942	1.6444	6.8378
$E_{t,r,s}$	-0.0108	0.6435	-4.6465	-0.4583	0.2344	0.4103	3.0797
$Y_{t-1,r,s}$	-0.0199	1.0739	-7.7921	-0.2339	-0.1666	-0.0903	18.1099
$\sigma_{t,r}^{GC^{LFI}}$	0.1271	0.2495	-1.3768	-0.0117	0.1606	0.2976	1.0912
C_r	-0.0096	0.3187	-3.1803	-0.1466	0.1033	0.1487	0.8699
$\sigma_{t,r}^{GC^{HCWI}}$	-0.0578	0.3941	-5.3486	-0.0720	0.0267	0.1294	1.0600
N_r	-0.0507	0.2850	-6.0159	-0.1472	-0.0878	-0.0090	5.9961
$\sigma_{t,r}^{LFI}$	0.0571	0.1880	-1.0218	-0.0774	0.0043	0.1869	1.7835
$H\bar{C}WI_{t,r}$	-0.0398	0.2728	-5.1760	-0.0401	0.0220	0.0603	4.9098
$\sigma_{t,r}^{GC^{HCWI}}$	-0.0397	0.2162	-3.5368	-0.0372	0.0072	0.0360	0.6820
			Sector C				
$G_{t-1,c}$	0.5076	1.6020	-4.3876	-0.6879	-0.1719	1.8570	32.7057
$Y_{t-1,r,s}$	-0.0799	4.4131	-2.7443	-0.4268	-0.3582	-0.2844	40.0018
$E_{t,r,s}$	0.0332	0.6940	-3.8163	-0.2809	0.1739	0.2772	10.1204
C_r	-0.0379	0.5979	-8.4955	-0.2638	0.1573	0.2204	1.8610
$\sigma_{t,r}^{GC^{LFI}}$	0.1295	0.3238	-1.6895	-0.0198	0.1964	0.3548	2.9479
N_r	-0.1256	0.7497	-1.1154	-0.2820	-0.1878	-0.0336	34.6550
$GC_{t,r}^{\bar{H}CWI}$	-0.0615	0.3468	-3.3417	-0.1883	0.0275	0.1578	3.1926
$\sigma_{t,r}^{LFI}$	0.0579	0.2174	-1.9379	-0.1138	0.0644	0.1743	1.8515
$\sigma_{t,r}^{GC^{HCWI}}$	0.0212	0.2196	-1.9955	0.0151	0.0500	0.0807	2.9653
$H\bar{C}WI_{t,r}$	-0.0093	0.2060	-3.7153	-0.0360	0.0171	0.0587	4.3897

Note: The table displays the descriptive statistics distribution of SHAP values for the top ten variables in the Random Forest Yearly Aggregations models. The variables are ordered by feature importance, where the variable with the largest predictive contributions listed first. Beeswarm and dependence plots are made available on request.
Source: Authors' calculations.

Table A.7: Distribution of Features' SHAP Values of Yearly Aggregations Climate Augmented XGBoost Models

	Mean	St.Dev.	Min.	25%	50%	75%	Max.
				Sector A			
$Y_{t-1,r,s}$	-0.1449	2.4827	-6.1502	-1.6527	-0.8217	0.6665	17.5841
$GC_{t,r}^{\bar{H}CWI}$	-0.0167	1.6774	-7.3773	-1.7764	0.9544	1.2684	4.8942
$G_{t-1,c}$	-0.2177	1.7592	-6.4769	-1.1513	-0.5965	1.1912	6.2085
N_r	0.0987	0.7438	-2.1093	-0.6581	0.3518	0.7004	2.9711
$\sigma_{t,r}^{GC^{HCWI}}$	-0.0300	0.4246	-1.1358	-0.2840	-0.1251	0.1807	1.9222
$HC\bar{W}I_{t,r}$	-0.0481	0.3746	-1.4699	-0.3935	0.0785	0.2436	1.5551
$\sigma_{t,r}^{GC^{LFI}}$	-0.0141	0.2910	-1.5423	-0.1712	0.0450	0.1505	1.5795
$E_{t,r,s}$	0.1021	4.2815	-2.3746	-0.1417	-0.0764	0.0552	27.8260
C_r	-0.0139	0.1869	-0.5823	-0.1624	0.0335	0.0818	0.8392
$S\bar{M}A_{t,r}$	0.0043	0.1791	-0.8656	0.0515	0.0673	0.0816	0.9959
				Sector B-E			
$G_{t-1,c}$	-0.0438	0.7483	-3.7170	-0.4184	-0.1896	0.2901	4.0269
$E_{t,r,s}$	-0.0210	0.2666	-1.1348	-0.2741	0.1081	0.1683	2.1072
$Y_{t-1,r,s}$	0.0041	0.4537	-1.4992	-0.1103	-0.0733	-0.0195	10.1444
$\sigma_{t,r}^{GC^{LFI}}$	-0.0144	0.1826	-1.2006	-0.0755	0.0282	0.1058	0.3841
N_r	0.0047	0.1816	-1.3240	-0.0805	-0.0358	0.0285	5.6483
C_r	-0.0091	0.1118	-0.4729	-0.0896	0.0418	0.0643	0.1654
$GC_{t,r}^{\bar{H}CWI}$	-0.0190	0.1423	-2.3388	-0.0553	0.0136	0.0635	0.3831
$HC\bar{W}I_{t,r}$	-0.0154	0.1492	-1.2956	-0.0294	0.0149	0.0481	0.5583
$\sigma_{t,r}^{LFI}$	-0.0057	0.0931	-1.0858	-0.0676	-0.0154	0.0635	0.9574
$\sigma_{t,r}^{GC^{HCWI}}$	-0.0065	0.1076	-0.9162	-0.0246	0.0149	0.0452	0.4470
				Sector C			
$G_{t-1,c}$	-0.0108	0.9171	-1.3095	-0.7836	-0.4142	1.2024	1.8631
$Y_{t-1,r,s}$	0.0380	2.0886	-0.1287	-0.1153	-0.1088	-0.1011	19.0713
$E_{t,r,s}$	0.0044	0.1190	-2.1394	-0.0083	0.0071	0.0173	0.8435
C_r	-0.0026	0.0455	-0.1520	-0.0512	0.0204	0.0254	0.0553
$GC_{t,r}^{\bar{H}CWI}$	-0.0021	0.0630	-0.3514	0.0074	0.0100	0.0130	0.2589
$\sigma_{t,r}^{HCWI}$	-0.0025	0.0229	-0.4963	-0.0058	-0.0010	0.0000	0.3490
$\sigma_{t,r}^{LFI}$	0.0013	0.0073	-0.1492	0.0019	0.0019	0.0019	0.0415
$\sigma_{t,r}^{GC^{HCWI}}$	-0.0004	0.0062	-0.2041	0.0000	0.0000	0.0000	0.0356
$\sigma_{t,r}^{GC^{LFI}}$	0.0001	0.0063	-0.2379	0.0000	0.0000	0.0000	0.2463
$HC\bar{W}I_{t,r}$	0.0001	0.0045	-0.0650	0.0000	0.0000	0.0000	0.1947

Note: The table displays the descriptive statistics distribution of SHAP values for the top ten variables in the XGBoost Yearly Aggregations models. The variables are ordered by feature importance, where the variable with the largest predictive contributions listed first. Beeswarm and dependence plots are made available on request.
Source: Authors' calculations.

Table A.8: Distribution of Features' SHAP Values of PCA-based Features Climate Augmented Random Forest Models

	Mean	St.Dev.	Min.	25%	50%	75%	Max.
			Sector A				
$Y_{t-1,r,s}$	-0.1360	2.9793	-10.6615	-2.2350	-0.5322	1.2640	19.0211
$G_{t-1,c}$	0.5322	1.8268	-8.0363	-0.6703	0.3266	0.9956	12.6568
$HCWI_{t,r}$	-0.6451	2.6382	-13.4811	-0.1727	0.1097	0.3152	22.9603
$N_{t,r}$	-0.2628	1.1118	-5.5620	-1.2002	0.2759	0.5553	12.0953
$EC_{t,r}$	-0.3394	1.2053	-7.4741	0.0280	0.1213	0.2031	1.5258
$LFI_{t,r}$	0.1646	1.5280	-8.7115	-0.2220	-0.1473	0.0154	48.7091
$SPI01_{t,r}$	-0.3163	0.7801	-2.5191	-0.5275	-0.3703	-0.2146	12.3063
$fAPAR_{t,r}$	0.2003	0.6288	-9.9501	-0.1835	0.2754	0.5222	9.2622
$SPI06_{t,r}$	-0.1596	0.5644	-3.7911	-0.3764	0.0570	0.1611	7.1965
$E_{t,r,s}$	0.1493	5.2149	-2.2559	-0.2715	-0.1502	0.0007	38.6088
			Sector B-E				
$G_{t-1,c}$	0.5903	1.3833	-1.9750	-0.5892	0.1831	1.7030	7.1729
$fAPAR_{t,r}$	0.2009	0.6365	-2.7796	-0.3270	0.2085	0.5348	3.3411
$E_{t,r,s}$	-0.0386	0.6115	-5.5273	-0.4654	0.2026	0.3423	2.2841
$Y_{t-1,r,s}$	-0.0220	0.9279	-4.0161	-0.2066	-0.1579	-0.0971	12.8513
$LFI_{t,r}$	0.0602	0.2640	-0.6882	-0.1679	0.0798	0.2816	1.1302
$C_{t,r}$	-0.0041	0.2951	-2.7518	-0.1868	0.1047	0.1399	1.2334
$SPI01_{t,r}$	-0.0968	0.1749	-1.2289	-0.1511	-0.0863	-0.0291	4.3310
$HCWI_{t,r}$	0.0050	0.1709	-3.6498	-0.0983	-0.0301	0.1077	1.0120
$N_{t,r}$	-0.0413	0.2194	-4.3793	-0.1098	-0.0626	0.0045	2.8517
$SPI12_{t,r}$	0.0822	0.1997	-0.3638	-0.0121	0.0074	0.0938	2.1641
			Sector C				
$G_{t-1,c}$	0.9706	2.3101	-4.7969	-0.5901	0.2550	2.1593	40.5768
$Y_{t-1,r,s}$	-0.1111	4.3891	-2.7621	-0.4455	-0.3652	-0.2847	33.8661
$SPI12_{t,r}$	0.3192	1.5564	-2.3163	-0.0314	-0.0050	0.2684	12.5665
$C_{t,r}$	-0.0398	0.7538	-12.4199	-0.3017	0.1920	0.2460	2.6986
$E_{t,r,s}$	0.0306	0.7070	-5.2438	-0.2758	0.1517	0.2547	9.1791
$fAPAR_{t,r}$	0.1578	0.4635	-1.5925	-0.2674	0.2529	0.4622	6.0178
$LFI_{t,r}$	0.1300	0.3855	-1.0218	-0.1835	0.1270	0.3639	2.9670
$N_{t,r}$	-0.1698	1.0695	-1.3488	-0.2616	-0.1838	-0.1032	49.1318
$SPI01_{t,r}$	-0.0976	0.4199	-4.3467	-0.2332	-0.1574	-0.0177	6.5049
$HCWI_{t,r}$	0.0622	0.2763	-1.1739	-0.1524	0.0215	0.2740	2.5869

Note: The table displays the descriptive statistics distribution of SHAP values for the top ten variables in the Random Forest PCA-based feature extraction climate augmented models. The variables are ordered by feature importance, where the variable with the largest predictive contributions listed first. Beeswarm and dependence plots are made available on request.
Source: Authors' calculations.

Table A.9: Distribution of Features' SHAP Values of PCA-based Features Climate Augmented XGBoost Models

	Mean	St.Dev.	Min.	25%	50%	75%	Max.
			Sector A				
$Y_{t-1,r,s}$	-0.1269	3.4154	-9.8479	-1.9307	-0.6346	0.8575	26.1503
$G_{t-1,c}$	-0.2434	1.9146	-7.9781	-1.4498	-0.7601	1.3242	7.9554
$HCWI_{t,r}$	-0.2044	1.9195	-16.2755	0.0466	0.2867	0.4993	13.0471
$N_{t,r}$	0.0954	1.5378	-3.4666	-0.6298	0.3383	0.5768	38.9335
$EC_{t,r}$	0.0649	0.6256	-2.6358	0.1749	0.2823	0.3884	1.1964
$SPI06_{t,r}$	0.0668	0.4632	-2.2627	-0.2886	0.1551	0.3956	2.3203
$SPI01_{t,r}$	-0.1458	0.7718	-1.8108	-0.3155	-0.1833	-0.0059	24.7799
$LFI_{t,r}$	0.0698	1.3360	-5.9729	-0.1674	-0.0855	0.0240	47.0724
$E_{t,r,s}$	0.5901	20.9602	-5.7511	-0.1633	-0.0224	0.0876	27.5884
$fAPAR_{t,r}$	-0.0055	0.4399	-1.2459	-0.2218	0.0485	0.1872	21.2725
			Sector B-E				
$G_{t-1,c}$	-0.0140	0.7309	-2.1907	-0.5100	-0.1052	0.3483	3.4105
$E_{t,r,s}$	-0.0167	0.2455	-1.2741	-0.2466	0.0907	0.1527	5.1455
$LFI_{t,r}$	-0.0055	0.2332	-0.8092	-0.1628	0.0674	0.1697	0.6833
$fAPAR_{t,r}$	0.0218	0.4001	-0.8880	-0.1369	-0.0554	0.0830	4.2926
$Y_{t-1,r,s}$	-0.0041	0.3740	-1.6657	-0.0859	-0.0538	-0.0187	7.7234
$C_{t,r}$	-0.0059	0.1490	-0.8234	-0.1688	0.0653	0.0826	0.2264
$HCWI_{t,r}$	-0.0169	0.1264	-1.5645	-0.0984	-0.0382	0.0603	0.4412
$N_{t,r}$	0.0113	0.1702	-1.9524	-0.0618	-0.0373	0.0107	4.5774
$SPI06_{t,r}$	-0.0063	0.1309	-0.6477	-0.0568	-0.0127	0.0495	0.7526
$SPI01_{t,r}$	-0.0080	0.1234	-0.8505	-0.0511	-0.0131	0.0391	1.4774
			Sector C				
$G_{t-1,c}$	-0.0592	1.0435	-3.9854	-0.8401	-0.3640	0.8883	5.5619
$Y_{t-1,r,s}$	0.0816	4.9427	-0.2440	-0.1091	-0.0897	-0.0511	11.8458
$E_{t,r,s}$	0.0210	0.3334	-1.8042	-0.0889	0.0750	0.0910	9.9018
$C_{t,r}$	-0.0096	0.1710	-3.0446	-0.1600	0.0717	0.0815	0.3944
$SPI12_{t,r}$	0.0411	0.2861	-2.9212	0.0013	0.0019	0.2046	0.2261
$fAPAR_{t,r}$	-0.0008	0.1032	-0.8122	-0.0927	-0.0048	0.0927	0.6813
$SPI06_{t,r}$	0.0176	0.1707	-4.4838	-0.0018	0.0375	0.0561	0.5781
$LFI_{t,r}$	-0.0075	0.0429	-0.2344	-0.0447	0.0061	0.0325	0.1124
$HCWI_{t,r}$	0.0017	0.0465	-1.2137	-0.0272	0.0131	0.0293	0.7334
$SPI01_{t,r}$	-0.0075	0.0451	-0.6570	-0.0251	-0.0138	0.0104	0.5130

Note: The table displays the descriptive statistics distribution of SHAP values for the top ten variables in the XGBoost PCA-based feature extraction climate augmented models. The variables are ordered by feature importance, where the variable with the largest predictive contributions listed first. Beeswarm and dependence plots are made available on request.
Source: Authors' calculations.

Table A.10: Distribution of Features' SHAP Values of MIDAS-based Features Climate Augmented Random Forest Models

	Mean	St.Dev.	Min.	25%	50%	75%	Max.
			Sector A				
$Y_{t-1,r,s}$	0.0202	4.2226	-16.8625	-2.3205	-1.2362	1.2695	36.3530
$G_{t-1,c}$	0.6791	2.6521	-12.7060	-0.7959	0.6030	1.9129	17.6895
$SPI06_{t,r}$	-0.6903	1.7439	-12.0173	-1.9947	0.2403	0.4507	1.3722
$N_{t,r}$	-0.2058	1.3972	-5.6848	-1.1328	0.2054	0.6646	17.8637
$HCWI_{t,r}$	-0.6044	1.3266	-6.9425	-1.1483	-0.4322	0.1473	8.4100
$SPI01_{t,r}$	-0.0059	1.4218	-1.6290	-0.5433	-0.3702	-0.1989	9.9315
$SMA_{t,r}$	-0.2713	0.6762	-3.6008	-0.3713	-0.0399	0.1185	3.5253
$E_{t,r,s}$	0.0982	2.8017	-1.8041	-0.2438	-0.0960	0.0784	49.4730
$LFI_{t,r}$	-0.1481	0.4068	-2.8758	-0.2514	-0.0200	0.0727	1.0743
$SPI12_{t,r}$	-0.0630	0.8642	-3.7823	-0.1086	-0.0191	0.0689	31.1602
			Sector B-E				
$G_{t-1,c}$	0.6020	1.4635	-2.3799	-0.6941	0.3916	1.7037	7.8167
$E_{t,r,s}$	-0.0350	0.6909	-7.0559	-0.4653	0.2194	0.3791	2.4418
$Y_{t-1,r,s}$	-0.0229	0.9722	-11.4670	-0.2067	-0.1551	-0.0931	19.4113
$LFI_{t,r}$	0.0957	0.3363	-1.2441	-0.1929	0.0316	0.4014	1.2491
$HCWI_{t,r}$	-0.1399	0.6417	-10.9690	-0.0951	0.0363	0.1168	3.7176
$C_{t,r}$	-0.0066	0.2883	-3.4278	-0.1521	0.0954	0.1387	0.8368
$SPI01_{t,r}$	0.0602	0.2715	-3.9326	-0.1092	0.0702	0.2056	2.2625
$N_{t,r}$	-0.0482	0.2867	-10.9668	-0.1395	-0.0850	0.0075	3.5414
$fAPAR_{t,r}$	-0.0446	0.2334	-1.2879	-0.1158	-0.0774	-0.0225	5.3526
$SPI12_{t,r}$	0.0660	0.2067	-1.1975	-0.0440	-0.0111	0.1162	1.9785
			Sector C				
$G_{t-1,c}$	1.3281	4.0436	-4.9291	-0.7238	0.1858	2.1392	32.8208
$SPI12_{t,r}$	0.7492	3.2998	-3.8452	-0.0402	-0.0019	0.4051	25.6674
$HCWI_{t,r}$	-0.1481	1.8229	-8.3525	-0.2806	0.0234	0.1286	15.3469
$Y_{t-1,r,s}$	-0.0719	3.7816	-2.7849	-0.4243	-0.3351	-0.2532	43.5235
$E_{t,r,s}$	0.0454	0.9061	-4.8422	-0.3246	0.1910	0.3406	17.4066
$SPI01_{t,r}$	0.1455	0.5820	-4.1377	-0.2188	0.0563	0.5429	5.4068
$C_{t,r}$	-0.0324	0.6392	-10.1083	-0.2379	0.1598	0.2346	2.7008
$LFI_{t,r}$	0.1585	0.5282	-1.3794	-0.2224	0.1961	0.3736	2.7803
$N_{t,r}$	-0.1479	0.6004	-1.1179	-0.2823	-0.1856	-0.0946	25.4317
$fAPAR_{t,r}$	-0.0008	0.5528	-3.1289	-0.1428	-0.0816	0.0307	17.6424

Note: The table displays the descriptive statistics distribution of SHAP values for the top ten variables in the Random Forest MIDAS-based feature extraction climate augmented models. The variables are ordered by feature importance, where the variable with the largest predictive contributions listed first. Beeswarm and dependence plots are made available on request.
Source: Authors' calculations.

Table A.11: Distribution of Features' SHAP Values of MIDAS-based Features Climate Augmented XGBoost Models

	Mean	St.Dev.	Min.	25%	50%	75%	Max.
			Sector A				
$G_{t-1,c}$	-0.1723	2.1887	-9.3027	-1.5354	-0.6558	1.5350	7.8610
$Y_{t-1,r,s}$	-0.0588	2.5795	-8.0837	-1.4738	-0.7157	0.6447	42.7552
$HCWI_{t,r}$	-0.0588	1.2967	-7.1211	-0.8750	0.0099	0.6429	13.3653
$SPI06_{t,r}$	0.2033	0.9635	-4.5615	-0.5844	0.5509	0.8818	7.6930
$N_{t,r}$	0.0902	0.6785	-2.7467	-0.4337	0.2069	0.5641	8.0740
$EC_{t,r}$	0.0858	0.6047	-2.4270	0.1848	0.3255	0.4428	1.3433
$SMA_{t,r}$	0.1123	0.5611	-1.6340	-0.2634	0.2320	0.5425	1.6270
$SPI01_{t,r}$	-0.0105	0.7324	-2.4746	-0.4049	-0.2114	0.0010	3.8471
$E_{t,r,s}$	0.2127	6.2662	-3.9026	-0.1335	0.0222	0.2129	13.6163
$SPI12_{t,r}$	0.0364	0.3605	-2.9811	-0.1137	0.1019	0.2422	3.0387
			Sector B-E				
$G_{t-1,c}$	-0.0802	2.2792	-2.7771	-1.3824	-0.7006	0.4146	15.3392
$LFI_{t,r}$	-0.0410	1.8738	-6.6539	-0.4658	-0.1889	1.0695	6.8767
$E_{t,r,s}$	-0.0237	0.3862	-4.3270	-0.2889	0.1360	0.1965	3.1568
$SPI01_{t,r}$	0.0225	0.5006	-1.2373	-0.0849	0.0315	0.1024	6.4398
$Y_{t-1,r,s}$	0.0051	0.4683	-1.0205	-0.1023	-0.0693	-0.0362	12.6726
$HCWI_{t,r}$	-0.0096	0.2488	-3.0636	0.0025	0.0296	0.0569	0.4938
$N_{t,r}$	0.0132	0.1564	-0.4734	-0.0511	-0.0296	0.0193	3.2646
$C_{t,r}$	-0.0094	0.0981	-1.2408	-0.0793	0.0292	0.0382	0.2752
$SPI06_{t,r}$	-0.0155	0.0893	-0.5059	-0.0508	-0.0150	0.0230	1.5317
$EC_{t,r}$	0.0000	0.0705	-0.3783	-0.0346	-0.0211	0.0373	0.9463
			Sector C				
$G_{t-1,c}$	0.0250	1.4537	-2.8662	-1.1942	-0.2126	1.6931	3.5260
$Y_{t-1,r,s}$	0.3253	21.7156	-0.2788	-0.1946	-0.1803	-0.1611	39.5993
$E_{t,r,s}$	0.0303	0.4499	-7.4076	-0.1423	0.1292	0.1451	5.4364
$C_{t,r}$	-0.0268	0.3238	-1.9222	-0.3108	0.1316	0.1343	0.7342
$HCWI_{t,r}$	-0.0109	0.2469	-5.3826	-0.0715	0.0796	0.0847	1.5222
$SPI01_{t,r}$	-0.0024	0.1458	-1.4070	-0.1050	-0.0877	0.1449	0.8758
$LFI_{t,r}$	-0.0106	0.1549	-1.6913	-0.2137	0.0804	0.0900	0.7381
$SPI06_{t,r}$	0.0015	0.0191	-0.1665	-0.0103	-0.0014	0.0020	0.1017
$fAPAR_{t,r}$	-0.0013	0.0290	-0.8482	-0.0102	-0.0102	0.0122	1.2464
$U_{t,r}$	-0.0003	0.0169	-0.0784	0.0075	0.0077	0.0080	0.0194

Note: The table displays the descriptive statistics distribution of SHAP values for the top ten variables in the XGBoost MIDAS-based feature extraction climate augmented models. The variables are ordered by feature importance, where the variable with the largest predictive contributions listed first. Beeswarm and dependence plots are made available on request.
Source: Authors' calculations.

Table A.12: Average Predictive Contributions within the Medians & St. Deviations Models

	Sector A			Sector B-E			Sector C		
	Linear Reg.	Random Forest	XGBoost	Linear Reg.	Random Forest	XGBoost	Linear Reg.	Random Forest	XGBoost
N_r	0.3762	-0.2410	-0.2014	0.1309	-0.0815	-0.0296	0.8213	-0.1562	-0.0076
$E_{t,r,s}$	0.4090	-0.0067	-0.0132	0.5282	0.0084	0.0069	0.0625	0.0293	0.0015
$Y_{t-1,r,s}$	-3.2126	-0.0185	-0.0508	-0.7985	-0.0037	-0.0026	-1.7310	-0.0390	-0.0137
$G_{t-1,c}$	-0.2522	0.0013	-0.0019	0.3931	-0.0358	-0.0194	0.1740	-0.0003	-0.0141
M_r	-0.8854	-0.0272	-0.0117	-0.4552	0.0008	0.0000	-0.6775	0.0016	0.0000
U_r	1.1929	0.0065	0.0003	-1.2317	0.0009	-0.0002	0.0689	0.0014	0.0000
R_r	-0.2779	0.0002	-0.0002	0.2580	-0.0001	0.0005	0.0533	0.0013	0.0000
C_r	-1.4417	-0.0065	0.0004	-0.8270	-0.0071	0.0002	-2.0727	-0.0283	-0.0003
$HCWI_{t,r}$	-4.8562	-0.0958	-0.0065	-1.9701	0.0053	0.0016	0.4587	0.0090	0.0005
$OwnRegion$	1.6550	-0.0063	0.0046	0.2470	0.0018	0.0017	-0.1015	0.0047	0.0001
$GC_{t,r}^{HCWI}$	-6.5112	-0.0895	-0.0111	-2.2171	0.0036	-0.0001	0.5602	0.0043	0.0004
$SPI01_{t,r}$	-1.0812	0.0000	0.0000	2.8646	-0.0002	0.0000	2.3341	-0.0001	0.0000
$OwnRegion$	1.8573	0.0000	0.0000	-4.2821	-0.0002	0.0000	-4.4634	-0.0002	0.0000
$GC_{t,r}^{SPI01}$	-2.9385	0.0000	0.0000	7.1468	0.0000	0.0000	6.7976	0.0001	0.0000
$SPI06_{t,r}$	7.5284	0.0254	0.0000	0.4315	0.0000	0.0001	0.1621	0.0006	0.0000
$OwnRegion$	3.2179	0.0251	0.0010	0.5592	0.0003	0.0000	0.0181	0.0008	0.0000
$GC_{t,r}^{SPI06}$	4.3105	0.0004	-0.0010	-0.1277	-0.0003	0.0001	0.1440	-0.0003	0.0000
$SPI12_{t,r}$	-2.2817	-0.0006	0.0068	0.3016	-0.0007	-0.0001	0.5485	-0.0027	0.0000
$OwnRegion$	-0.9168	0.0013	0.0071	0.2562	-0.0004	0.0002	0.2799	-0.0021	0.0000
$GC_{t,r}^{SPI12}$	-1.3649	-0.0019	-0.0002	0.0455	-0.0003	-0.0004	0.2686	-0.0007	0.0000
$LFI_{t,r}$	-18.3530	0.1007	0.0392	16.2342	0.0169	0.0023	15.1460	0.0194	0.0000
$OwnRegion$	-6.7037	0.0433	0.0111	4.7357	0.0059	0.0014	6.7405	0.0116	0.0001
$GC_{t,r}^{LFI}$	-11.6493	0.0573	0.0281	11.4985	0.0109	0.0010	8.4055	0.0079	0.0000
$SMA_{t,r}$	3.0591	0.0074	0.0061	0.5488	-0.0005	0.0002	0.8182	-0.0007	0.0000
$FAPAR_{t,r}$	-12.1011	-0.0075	-0.0083	0.5397	0.0004	0.0001	1.0788	-0.0002	0.0000
$EC_{t,r}$	-11.7883	0.0000	0.0000	-137.8228	0.0000	0.0001	-114.0757	0.0000	0.0000
$EC_{t,r}^{01}$	-3.9294	0.0000	0.0000	-45.9409	0.0000	0.0000	-38.0252	0.0000	0.0000
$EC_{t,r}^{06}$	-3.9294	0.0000	0.0000	-45.9409	0.0000	0.0000	-38.0252	0.0000	0.0000
$EC_{t,r}^{12}$	-3.9294	0.0000	0.0000	-45.9409	0.0000	0.0000	-38.0252	0.0000	0.0000

Note: The table presents the average contributions to predicted outcomes across all models utilising yearly medians and standard deviations. For linear models, regression coefficients are reported, while for ML models, the average SHAP values are used to quantify feature importance. Heat wave and drought values are represented by the sum of the coefficients, or SHAP values, of median and standard deviation variables. Climate-related features are decomposed into own region, geographic compounding, and event compounding types (highlighted in blue).
Source: Authors' calculations.

Table A.13: Average Predictive Contributions within PCA-based Features Extraction Models

	Sector A			Sector B-E			Sector C		
	Linear Reg.	Random Forest	XGBoost	Linear Reg.	Random Forest	XGBoost	Linear Reg.	Random Forest	XGBoost
N_r	-4.0549	-0.2976	-0.1316	-0.8570	-0.0653	-0.0269	-1.7629	-0.1504	-0.0141
$E_{t,r,s}$	0.5007	0.0383	0.0024	0.5082	-0.0036	0.0044	0.0446	0.0253	0.0113
$Y_{t-1,r,s}$	-0.8888	0.0491	-0.0010	0.3444	-0.0026	0.0000	0.1142	-0.0398	-0.0115
$G_{t-1,c}$	0.7968	-0.0842	-0.1136	0.1441	-0.0347	0.0088	0.8340	0.0374	-0.0197
M_r	-1.4326	0.0028	-0.0024	-0.6199	0.0005	0.0002	-0.8922	0.0023	0.0000
U_r	1.1591	0.0019	0.0013	-1.1642	0.0008	0.0006	0.1257	0.0053	0.0000
R_r	-0.2013	0.0007	-0.0003	0.2456	-0.0004	0.0003	0.0246	0.0016	0.0001
C_r	-1.7584	-0.0010	0.0039	-0.8752	-0.0035	0.0002	-2.1044	-0.0283	-0.0018
$HCWI_{t,r}$	-0.7032	-0.0584	-0.0074	0.0148	-0.0031	-0.0064	0.0821	-0.0014	-0.0014
$OwnRegion$	-0.3692	-0.0307	-0.0039	0.0078	-0.0016	-0.0034	0.0430	-0.0007	-0.0008
$GC_{t,r}^{HCWI}$	-0.3340	-0.0278	-0.0035	0.0070	-0.0015	-0.0031	0.0392	-0.0007	-0.0007
$SPI01_{t,r}$	2.8046	0.0187	0.0249	0.6473	-0.0174	-0.0101	0.8969	-0.0174	-0.0025
$OwnRegion$	1.3798	0.0092	0.0122	0.3185	-0.0085	-0.0050	0.4413	-0.0085	-0.0012
$GC_{t,r}^{SPI01}$	1.4248	0.0095	0.0126	0.3288	-0.0088	-0.0051	0.4556	-0.0089	-0.0013
$SPI06_{t,r}$	-1.9742	0.0264	0.0055	-0.7002	0.0022	-0.0054	-0.9495	0.0218	0.0039
$OwnRegion$	-1.0172	0.0136	0.0028	-0.3615	0.0011	-0.0028	-0.4857	0.0111	0.0020
$GC_{t,r}^{SPI06}$	-0.9570	0.0129	0.0026	-0.3386	0.0011	-0.0026	-0.4638	0.0106	0.0019
$SPI12_{t,r}$	0.9908	-0.0217	-0.0296	0.2678	0.0171	0.0029	0.4289	-0.0456	0.0098
$OwnRegion$	0.5307	-0.0116	-0.0159	0.1444	0.0092	0.0016	0.2299	-0.0244	0.0053
$GC_{t,r}^{SPI12}$	0.4601	-0.0101	-0.0138	0.1233	0.0080	0.0013	0.1990	-0.0211	0.0045
$LFI_{t,r}$	9.1629	-0.0085	0.0174	1.6230	0.0081	0.0056	1.4679	0.0193	0.0023
$OwnRegion$	5.0917	-0.0047	0.0097	0.9098	0.0045	0.0031	0.8130	0.0107	0.0013
$GC_{t,r}$	4.0712	-0.0038	0.0077	0.7133	0.0036	0.0025	0.6549	0.0086	0.0010
$SMA_{t,r}$	-0.2708	0.0239	0.0287	0.0422	0.0030	-0.0022	-0.0149	0.0069	0.0013
$FAPAR_{t,r}$	-0.9959	0.0864	0.0658	0.3970	0.0352	0.0122	0.1610	0.0445	0.0086
$EC_{t,r}$	-18.9298	-0.0021	0.0012	1.0696	0.0049	0.0027	2.2196	0.0070	0.0005
$EC_{t,r}^{01}$	-9.1976	-0.0010	0.0006	0.5171	0.0024	0.0013	1.0817	0.0034	0.0002
$EC_{t,r}^{06}$	-7.1517	-0.0008	0.0005	0.4060	0.0018	0.0010	0.8375	0.0026	0.0002
$EC_{t,t}^{12}$	-2.5805	-0.0003	0.0002	0.1465	0.0007	0.0004	0.3004	0.0009	0.0001

Note: The table presents the average contributions to predicted outcomes across all models utilising PCA-based feature extraction. For linear models, regression coefficients are reported, while for ML models, the average SHAP values are used to quantify feature importance. Climate-related features are decomposed into own region, geographic compounding, and event compounding types (highlighted in blue), based on factor loadings derived from the PCA kernel.
Source: Authors' calculations.

Table A.14: Average Predictive Contributions within MIDAS-based Features Extraction Models

	Sector A			Sector B-E			Sector C		
	Linear Reg.	Random Forest	XGBoost	Linear Reg.	Random Forest	XGBoost	Linear Reg.	Random Forest	XGBoost
N_r	-3.5201	-0.2815	-0.2119	-0.8314	-0.0726	-0.0270	-1.7328	-0.1662	0.0040
$E_{t,r,s}$	0.2516	0.0480	0.0063	0.5049	0.0038	0.0085	0.0215	0.0284	0.0097
$Y_{t-1,r,s}$	-0.5562	-0.0203	-0.0291	0.3968	-0.0032	-0.0068	0.2238	-0.0350	-0.0181
$G_{t-1,c}$	0.4901	-0.0569	-0.1521	0.1510	-0.0324	0.0025	0.8092	0.0384	-0.0089
M_r	-0.7923	-0.0054	0.0012	-0.2416	0.0011	-0.0001	-0.4998	0.0033	0.0000
U_r	1.1793	0.0030	0.0024	-1.2466	0.0015	0.0008	0.0199	0.0013	-0.0001
R_r	-0.0926	0.0013	0.0012	0.2726	0.0006	0.0000	0.0238	0.0017	0.0000
C_r	-1.8548	-0.0040	0.0038	-0.8945	-0.0051	-0.0008	-2.0580	-0.0256	-0.0227
$HCWI_{t,r}$	0.7173	-0.0470	0.0085	1.1375	0.0064	-0.0006	1.0037	0.0309	0.0074
$OwnRegion$	0.6388	-0.0419	0.0069	0.2571	0.0020	-0.0001	0.1099	0.0155	0.0049
$GC_{t,r}^{HCWI}$	0.0785	-0.0051	0.0016	0.8803	0.0044	-0.0006	0.8939	0.0155	0.0025
$SPI01_{t,r}$	3.1600	-0.0647	-0.0311	0.7348	-0.0015	-0.0053	0.8004	-0.0015	-0.0036
$OwnRegion$	2.8142	-0.0576	-0.0252	0.6543	-0.0013	-0.0043	0.7128	-0.0014	-0.0029
$GC_{t,r}^{SPI01}$	0.3459	-0.0071	-0.0058	0.0804	-0.0002	-0.0010	0.0876	-0.0002	-0.0007
$SPI06_{t,r}$	1.2569	-0.0129	0.0297	-5.7149	0.0037	-0.0015	5.7065	-0.0040	-0.0053
$OwnRegion$	1.1193	-0.0115	0.0241	-1.2918	0.0012	-0.0002	0.6246	-0.0020	-0.0035
$GC_{t,r}^{SPI06}$	0.1376	-0.0014	0.0056	-4.4231	0.0026	-0.0013	5.0819	-0.0020	-0.0018
$SPI12_{t,r}$	-0.3859	0.0043	0.0036	1.2962	0.0003	0.0007	20.8891	-0.0364	-0.0005
$OwnRegion$	-0.3437	0.0038	0.0029	0.2930	0.0001	0.0001	2.2863	-0.0182	-0.0004
$GC_{t,r}^{SPI12}$	-0.0422	0.0005	0.0007	1.0032	0.0002	0.0006	18.6029	-0.0182	-0.0002
$LFI_{t,r}$	0.2515	0.0074	-0.0100	0.8496	0.0136	-0.0033	1.0232	0.0290	0.0104
$OwnRegion$	0.2240	0.0066	-0.0081	0.1921	0.0043	-0.0004	0.1120	0.0145	0.0068
$GC_{t,r}^{LFI}$	0.0275	0.0008	-0.0019	0.6576	0.0093	-0.0029	0.9112	0.0145	0.0036
$SMA_{t,r}$	0.7121	0.0316	0.0250	0.6634	-0.0001	-0.0010	1.3874	-0.0090	0.0000
$FAPAR_{t,r}$	1.9427	0.0126	0.0339	0.7422	0.0066	0.0070	0.6416	0.0020	0.0011
$EC_{t,r}$	0.2448	0.0032	0.0095	12.1794	0.0037	0.0031	-4.7344	0.0039	-0.0001
$EC_{t,r}^{01}$	0.1564	0.0020	0.0050	0.5165	0.0004	0.0001	-0.0788	0.0010	0.0000
$EC_{t,r}^{06}$	0.0843	0.0011	0.0041	6.5674	0.0018	0.0011	-1.6312	0.0019	-0.0001
$EC_{t,r}^{12}$	0.0041	0.0001	0.0004	5.0955	0.0015	0.0020	-3.0245	0.0010	0.0000

Note: The table presents the average contributions to predicted outcomes across all models utilising MIDAS-based feature extraction. For linear models, regression coefficients are reported, while for ML models, the average SHAP values are used to quantify feature importance. Climate-related features are decomposed into own region, geographic compounding, and event compounding types (highlighted in blue), based on factor loadings derived from the beta polynomial function.
Source: Authors' calculations.

Table A.15: Average Predictive Contributions within PCA Features Extraction Models by Seasons

	Sector A			Sector B-E			Sector C		
	Linear Regression	Random Forest	XGBoost	Linear Regression	Random Forest	XGBoost	Linear Regression	Random Forest	XGBoost
$HCWI_{t,r}$	-0.7032	-0.0584	-0.0074	0.0148	-0.0031	-0.0064	0.0821	-0.0014	-0.0014
OwnRegion	-0.3692	-0.0307	-0.0039	0.0078	-0.0016	-0.0034	0.0430	-0.0007	-0.0008
Winter	-0.0341	-0.0030	-0.0004	0.0006	-0.0001	-0.0003	0.0038	-0.0001	0.0000
Spring	-0.0211	-0.0017	-0.0002	0.0005	-0.0001	-0.0002	0.0024	0.0000	0.0000
Summer	-0.1938	-0.0160	-0.0020	0.0042	-0.0009	-0.0018	0.0228	-0.0004	-0.0004
Autumn	-0.1202	-0.0100	-0.0013	0.0024	-0.0005	-0.0011	0.0140	-0.0002	-0.0002
$GC_{t,r}^{HCWI}$	-0.3340	-0.0278	-0.0035	0.0070	-0.0015	-0.0031	0.0392	-0.0007	-0.0007
Winter	-0.0309	-0.0026	-0.0003	0.0005	-0.0001	-0.0002	0.0035	-0.0001	-0.0001
Spring	-0.0128	-0.0010	-0.0001	0.0003	-0.0001	-0.0001	0.0015	0.0000	0.0000
Summer	-0.1796	-0.0148	-0.0019	0.0039	-0.0008	-0.0017	0.0213	-0.0004	-0.0004
Autumn	-0.1107	-0.0093	-0.0012	0.0022	-0.0005	-0.0010	0.0129	-0.0002	-0.0002
$SPI01_{t,r}$	2.8046	0.0187	0.0249	0.6473	-0.0174	-0.0101	0.8969	-0.0174	-0.0025
OwnRegion	1.3798	0.0092	0.0122	0.3185	-0.0085	-0.0050	0.4413	-0.0085	-0.0012
Winter	0.0019	0.0000	0.0000	0.0010	0.0000	0.0000	0.0010	0.0000	0.0000
Spring	0.5499	0.0037	0.0049	0.1268	-0.0034	-0.0020	0.1754	-0.0034	-0.0005
Summer	-0.0291	-0.0002	-0.0003	-0.0058	0.0002	0.0001	-0.0097	0.0002	0.0000
Autumn	0.8572	0.0057	0.0076	0.1985	-0.0053	-0.0031	0.2746	-0.0053	-0.0008
$GC_{t,r}^{SPI01}$	1.4248	0.0095	0.0126	0.3288	-0.0088	-0.0051	0.4556	-0.0089	-0.0013
Winter	-0.0036	0.0000	0.0000	-0.0009	0.0000	0.0000	-0.0005	0.0000	0.0000
Spring	0.5743	0.0038	0.0051	0.1311	-0.0035	-0.0021	0.1827	-0.0035	-0.0005
Summer	-0.0270	-0.0002	-0.0002	-0.0058	0.0002	0.0001	-0.0085	0.0002	0.0000
Autumn	0.8811	0.0059	0.0078	0.2025	-0.0055	-0.0032	0.2818	-0.0055	-0.0008
$SPI06_{t,r}$	-1.9742	0.0264	0.0055	-0.7002	0.0022	-0.0054	-0.9495	0.0218	0.0039
OwnRegion	-1.0172	0.0136	0.0028	-0.3615	0.0011	-0.0028	-0.4857	0.0111	0.0020
Winter	-0.1638	0.0022	0.0005	-0.0585	0.0002	-0.0005	-0.0828	0.0019	0.0003
Spring	-0.1212	0.0019	0.0003	-0.0540	0.0002	-0.0004	-0.0772	0.0018	0.0003
Summer	-0.3685	0.0049	0.0010	-0.1302	0.0004	-0.0010	-0.1705	0.0039	0.0007
Autumn	-0.3637	0.0045	0.0010	-0.1188	0.0004	-0.0009	-0.1551	0.0036	0.0007
$GC_{t,r}^{SPI06}$	-0.9570	0.0129	0.0026	-0.3386	0.0011	-0.0026	-0.4638	0.0106	0.0019
Winter	-0.1565	0.0021	0.0004	-0.0562	0.0002	-0.0004	-0.0798	0.0018	0.0003
Spring	-0.1091	0.0018	0.0003	-0.0483	0.0002	-0.0004	-0.0713	0.0016	0.0003
Summer	-0.3521	0.0047	0.0010	-0.1234	0.0004	-0.0009	-0.1655	0.0038	0.0007
Autumn	-0.3393	0.0043	0.0009	-0.1107	0.0003	-0.0008	-0.1471	0.0034	0.0006
$SPI12_{t,r}$	0.9908	-0.0217	-0.0296	0.2678	0.0171	0.0029	0.4289	-0.0456	0.0098
OwnRegion	0.5307	-0.0116	-0.0159	0.1444	0.0092	0.0016	0.2299	-0.0244	0.0053
Winter	0.1222	-0.0027	-0.0037	0.0335	0.0021	0.0004	0.0526	-0.0056	0.0013
Spring	0.1567	-0.0034	-0.0047	0.0432	0.0027	0.0005	0.0684	-0.0073	0.0016
Summer	0.1526	-0.0034	-0.0046	0.0411	0.0026	0.0004	0.0664	-0.0071	0.0015
Autumn	0.0992	-0.0022	-0.0030	0.0266	0.0017	0.0003	0.0425	-0.0045	0.0009
$GC_{t,r}^{SPI12}$	0.4601	-0.0101	-0.0138	0.1233	0.0080	0.0013	0.1990	-0.0211	0.0045
Winter	0.1090	-0.0024	-0.0033	0.0293	0.0019	0.0003	0.0467	-0.0050	0.0011
Spring	0.1365	-0.0030	-0.0041	0.0370	0.0024	0.0004	0.0595	-0.0063	0.0014
Summer	0.1322	-0.0029	-0.0040	0.0352	0.0023	0.0004	0.0575	-0.0061	0.0013
Autumn	0.0824	-0.0018	-0.0025	0.0218	0.0014	0.0002	0.0353	-0.0037	0.0008

Note: This table continues on the next page.

	Sector A			Sector B-E			Sector C		
	Linear Regression	Random Forest	XGBoost	Linear Regression	Random Forest	XGBoost	Linear Regression	Random Forest	XGBoost
$LFI_{t,r}$	9.1629	-0.0085	0.0174	1.6230	0.0081	0.0056	1.4679	0.0193	0.0023
$OwnRegion$	5.0917	-0.0047	0.0097	0.9098	0.0045	0.0031	0.8130	0.0107	0.0013
Winter	1.2850	-0.0012	0.0024	0.2228	0.0012	0.0008	0.2121	0.0028	0.0003
Spring	1.7643	-0.0016	0.0034	0.3080	0.0015	0.0011	0.2736	0.0036	0.0004
Summer	1.4473	-0.0013	0.0028	0.2688	0.0013	0.0009	0.2321	0.0031	0.0004
Autumn	0.5951	-0.0006	0.0011	0.1102	0.0005	0.0004	0.0952	0.0013	0.0001
$GC_{t,r}^{LFI}$	4.0712	-0.0038	0.0077	0.7133	0.0036	0.0025	0.6549	0.0086	0.0010
Winter	1.1092	-0.0010	0.0021	0.1883	0.0010	0.0007	0.1839	0.0024	0.0003
Spring	1.4161	-0.0013	0.0027	0.2435	0.0012	0.0009	0.2217	0.0029	0.0003
Summer	1.1136	-0.0010	0.0021	0.2023	0.0010	0.0007	0.1790	0.0024	0.0003
Autumn	0.4323	-0.0004	0.0008	0.0792	0.0004	0.0003	0.0703	0.0009	0.0001
$SMA_{t,r}$	-0.2708	0.0239	0.0287	0.0422	0.0030	-0.0022	-0.0149	0.0069	0.0013
Winter	-0.1033	0.0091	0.0109	0.0161	0.0012	-0.0008	-0.0057	0.0027	0.0005
Spring	-0.1187	0.0105	0.0126	0.0187	0.0013	-0.0010	-0.0066	0.0031	0.0006
Summer	-0.0360	0.0032	0.0038	0.0056	0.0004	-0.0003	-0.0020	0.0009	0.0002
Autumn	-0.0128	0.0011	0.0014	0.0017	0.0001	-0.0001	-0.0006	0.0003	0.0001
$FAPAR_{t,r}$	-0.9959	0.0864	0.0658	0.3970	0.0352	0.0122	0.1610	0.0445	0.0086
Winter	-0.5136	0.0444	0.0339	0.2063	0.0180	0.0062	0.0824	0.0228	0.0045
Spring	-0.2011	0.0175	0.0133	0.0800	0.0072	0.0025	0.0333	0.0092	0.0017
Summer	-0.0524	0.0046	0.0035	0.0212	0.0019	0.0007	0.0085	0.0024	0.0004
Autumn	-0.2287	0.0198	0.0151	0.0894	0.0081	0.0028	0.0368	0.0102	0.0019
$EC_{t,r}$	-18.9298	-0.0021	0.0012	1.0696	0.0049	0.0027	2.2196	0.0070	0.0005
$EC_{t,r}^{01}$	-9.1976	-0.0010	0.0006	0.5171	0.0024	0.0013	1.0817	0.0034	0.0002
Winter	-0.0862	0.0000	0.0000	0.0046	0.0000	0.0000	0.0097	0.0000	0.0000
Spring	-1.0388	-0.0001	0.0001	0.0565	0.0003	0.0002	0.1242	0.0004	0.0000
Summer	-7.4896	-0.0008	0.0005	0.4144	0.0019	0.0011	0.8814	0.0028	0.0002
Autumn	-0.5830	-0.0001	0.0000	0.0416	0.0002	0.0001	0.0665	0.0002	0.0000
$EC_{t,r}^{06}$	-7.1517	-0.0008	0.0005	0.4060	0.0018	0.0010	0.8375	0.0026	0.0002
Winter	-0.6034	-0.0001	0.0000	0.0339	0.0002	0.0001	0.0703	0.0002	0.0000
Spring	-0.1492	0.0000	0.0000	0.0083	0.0000	0.0000	0.0172	0.0001	0.0000
Summer	-5.0747	-0.0006	0.0003	0.2859	0.0013	0.0007	0.5955	0.0019	0.0001
Autumn	-1.3244	-0.0001	0.0001	0.0779	0.0003	0.0002	0.1545	0.0005	0.0000
$EC_{t,r}^{12}$	-2.5805	-0.0003	0.0002	0.1465	0.0007	0.0004	0.3004	0.0009	0.0001
Winter	-0.5465	-0.0001	0.0000	0.0310	0.0001	0.0001	0.0632	0.0002	0.0000
Spring	-0.1035	0.0000	0.0000	0.0055	0.0000	0.0000	0.0118	0.0000	0.0000
Summer	-1.0219	-0.0001	0.0001	0.0557	0.0003	0.0001	0.1193	0.0004	0.0000
Autumn	-0.9085	-0.0001	0.0001	0.0543	0.0002	0.0001	0.1061	0.0003	0.0000

Note: The table presents the average contributions of climate features to predicted outcomes across all models utilising PCA-based feature extraction. For linear models, regression coefficients are reported, while for ML models, the average SHAP values are used to quantify feature importance. Climate-related features are shown with headline contributions (highlighted in grey), decomposed into own region, geographic compounding, and event compounding types (highlighted in blue), and further decomposed by seasonality, based on factor loadings derived.
Source: Authors' calculations.

Table A.16: Average Predictive Contributions within MIDAS Features Extraction Models by Seasons

	Sector A			Sector B-E			Sector C		
	Linear Regression	Random Forest	XGBoost	Linear Regression	Random Forest	XGBoost	Linear Regression	Random Forest	XGBoost
$HCWI_{t,r}$	0.7173	-0.0470	0.0085	1.1375	0.0064	-0.0006	1.0037	0.0309	0.0074
OwnRegion	0.6388	-0.0419	0.0069	0.2571	0.0020	-0.0001	0.1099	0.0155	0.0049
Winter	0.0675	-0.0044	0.0008	0.0740	0.0004	0.0000	0.0359	0.0024	0.0007
Spring	0.2031	-0.0133	0.0019	0.0046	0.0002	0.0000	0.0014	0.0027	0.0007
Summer	0.2169	-0.0142	0.0023	0.0418	0.0005	0.0000	0.0147	0.0046	0.0016
Autumn	0.1514	-0.0099	0.0020	0.1367	0.0009	0.0000	0.0579	0.0057	0.0020
$GC_{t,r}^{HCWI}$	0.0785	-0.0051	0.0016	0.8803	0.0044	-0.0006	0.8939	0.0155	0.0025
Winter	0.0446	-0.0029	0.0008	0.1882	0.0009	-0.0001	0.1050	0.0040	0.0011
Spring	0.0280	-0.0018	0.0006	0.3355	0.0015	-0.0002	0.2472	0.0055	0.0010
Summer	0.0056	-0.0004	0.0002	0.2707	0.0013	-0.0002	0.3162	0.0041	0.0004
Autumn	0.0003	0.0000	0.0000	0.0860	0.0007	-0.0001	0.2255	0.0019	0.0000
$SPI01_{t,r}$	3.1600	-0.0647	-0.0311	0.7348	-0.0015	-0.0053	0.8004	-0.0015	-0.0036
OwnRegion	2.8142	-0.0576	-0.0252	0.6543	-0.0013	-0.0043	0.7128	-0.0014	-0.0029
Winter	0.2975	-0.0061	-0.0029	0.0478	-0.0001	-0.0002	0.0286	-0.0001	-0.0003
Spring	0.8945	-0.0183	-0.0068	0.0030	0.0000	0.0000	0.0011	-0.0001	-0.0003
Summer	0.9553	-0.0196	-0.0085	0.0270	-0.0001	-0.0001	0.0117	-0.0002	-0.0008
Autumn	0.6668	-0.0137	-0.0071	0.0883	-0.0002	-0.0003	0.0462	-0.0003	-0.0009
$GC_{t,r}^{SPI01}$	0.3459	-0.0071	-0.0058	0.0804	-0.0002	-0.0010	0.0876	-0.0002	-0.0007
Winter	0.1967	-0.0040	-0.0028	0.1216	-0.0002	-0.0006	0.0837	-0.0002	-0.0005
Spring	0.1234	-0.0025	-0.0023	0.2167	-0.0003	-0.0013	0.1971	-0.0003	-0.0005
Summer	0.0245	-0.0005	-0.0007	0.1748	-0.0003	-0.0017	0.2522	-0.0002	-0.0002
Autumn	0.0013	0.0000	-0.0001	0.0556	-0.0002	-0.0012	0.1798	-0.0001	0.0000
$SPI06_{t,r}$	1.2569	-0.0129	0.0297	-5.7149	0.0037	-0.0015	5.7065	-0.0040	-0.0053
OwnRegion	1.1193	-0.0115	0.0241	-1.2918	0.0012	-0.0002	0.6246	-0.0020	-0.0035
Winter	0.1183	-0.0012	0.0027	-0.3717	0.0002	-0.0001	0.2042	-0.0003	-0.0005
Spring	0.3558	-0.0036	0.0065	-0.0232	0.0001	0.0000	0.0079	-0.0004	-0.0005
Summer	0.3800	-0.0039	0.0081	-0.2100	0.0003	0.0000	0.0833	-0.0006	-0.0011
Autumn	0.2652	-0.0027	0.0068	-0.6869	0.0005	-0.0001	0.3292	-0.0007	-0.0014
$GC_{t,r}^{SPI06}$	0.1376	-0.0014	0.0056	-4.4231	0.0026	-0.0013	5.0819	-0.0020	-0.0018
Winter	0.0782	-0.0008	0.0027	-0.9456	0.0005	-0.0002	0.5969	-0.0005	-0.0008
Spring	0.0491	-0.0005	0.0022	-1.6854	0.0009	-0.0004	1.4053	-0.0007	-0.0007
Summer	0.0098	-0.0001	0.0007	-1.3599	0.0008	-0.0005	1.7978	-0.0005	-0.0003
Autumn	0.0005	0.0000	0.0001	-0.4322	0.0004	-0.0003	1.2819	-0.0002	0.0000
$SPI12_{t,r}$	-0.3859	0.0043	0.0036	1.2962	0.0003	0.0007	20.8891	-0.0364	-0.0005
OwnRegion	-0.3437	0.0038	0.0029	0.2930	0.0001	0.0001	2.2863	-0.0182	-0.0004
Winter	-0.0363	0.0004	0.0003	0.0843	0.0000	0.0000	0.7474	-0.0028	0.0000
Spring	-0.1092	0.0012	0.0008	0.0053	0.0000	0.0000	0.0290	-0.0032	0.0000
Summer	-0.1167	0.0013	0.0010	0.0476	0.0000	0.0000	0.3050	-0.0055	-0.0001
Autumn	-0.0814	0.0009	0.0008	0.1558	0.0000	0.0000	1.2049	-0.0068	-0.0001
$GC_{t,r}^{SPI12}$	-0.0422	0.0005	0.0007	1.0032	0.0002	0.0006	18.6029	-0.0182	-0.0002
Winter	-0.0240	0.0003	0.0003	0.2145	0.0000	0.0001	2.1850	-0.0047	-0.0001
Spring	-0.0151	0.0002	0.0003	0.3823	0.0001	0.0002	5.1444	-0.0064	-0.0001
Summer	-0.0030	0.0000	0.0001	0.3084	0.0001	0.0002	6.5811	-0.0048	0.0000
Autumn	-0.0002	0.0000	0.0000	0.0980	0.0000	0.0002	4.6923	-0.0022	0.0000

Note: This table continues on the next page.

	Sector A			Sector B-E			Sector C		
	Linear Regression	Random Forest	XGBoost	Linear Regression	Random Forest	XGBoost	Linear Regression	Random Forest	XGBoost
$LFI_{t,r}$	0.2515	0.0074	-0.0100	0.8496	0.0136	-0.0033	1.0232	0.0290	0.0104
$OwnRegion$	0.2240	0.0066	-0.0081	0.1921	0.0043	-0.0004	0.1120	0.0145	0.0068
Winter	0.0237	0.0007	-0.0009	0.0553	0.0009	-0.0001	0.0366	0.0022	0.0009
Spring	0.0712	0.0021	-0.0022	0.0035	0.0003	0.0000	0.0014	0.0026	0.0009
Summer	0.0760	0.0022	-0.0027	0.0312	0.0011	0.0000	0.0149	0.0044	0.0022
Autumn	0.0531	0.0016	-0.0023	0.1021	0.0020	-0.0002	0.0590	0.0054	0.0028
$GC_{t,r}^{LFI}$	0.0275	0.0008	-0.0019	0.6576	0.0093	-0.0029	0.9112	0.0145	0.0036
Winter	0.0157	0.0005	-0.0009	0.1406	0.0019	-0.0003	0.1070	0.0038	0.0015
Spring	0.0098	0.0003	-0.0007	0.2506	0.0031	-0.0008	0.2520	0.0051	0.0015
Summer	0.0098	0.0003	-0.0007	0.2022	0.0028	-0.0010	0.3224	0.0038	0.0005
Autumn	0.0001	0.0000	0.0000	0.0643	0.0015	-0.0007	0.2298	0.0018	0.0001
$SMA_{t,r}$	0.7121	0.0316	0.0250	0.6634	-0.0001	-0.0010	1.3874	-0.0090	0.0000
Winter	0.1231	0.0055	0.0031	0.0004	0.0000	0.0000	0.0002	-0.0004	0.0000
Spring	0.4311	0.0191	0.0137	0.0680	0.0000	0.0000	0.0620	-0.0029	0.0000
Summer	0.1480	0.0066	0.0072	0.3336	0.0000	-0.0004	0.4758	-0.0036	0.0000
Autumn	0.0099	0.0004	0.0009	0.2614	0.0000	-0.0006	0.8494	-0.0021	0.0000
$FAPAR_{t,r}$	1.9427	0.0126	0.0339	0.7422	0.0066	0.0070	0.6416	0.0020	0.0011
Winter	0.3359	0.0022	0.0043	0.0004	0.0001	0.0000	0.0001	0.0001	0.0000
Spring	1.1761	0.0076	0.0187	0.0761	0.0012	0.0003	0.0287	0.0007	0.0005
Summer	0.4038	0.0026	0.0097	0.3733	0.0029	0.0024	0.2200	0.0008	0.0005
Autumn	0.0269	0.0002	0.0013	0.2924	0.0025	0.0043	0.3928	0.0005	0.0001
$EC_{t,r}$	0.2448	0.0032	0.0095	12.1794	0.0037	0.0031	-4.7344	0.0039	-0.0001
$EC_{t,r}^{01}$	0.1564	0.0020	0.0050	0.5165	0.0004	0.0001	-0.0788	0.0010	0.0000
Winter	0.0335	0.0004	0.0011	0.1475	0.0001	0.0000	-0.0218	0.0002	0.0000
Spring	0.0377	0.0005	0.0012	0.1262	0.0001	0.0000	-0.0196	0.0002	0.0000
Summer	0.0478	0.0006	0.0016	0.2005	0.0001	0.0000	-0.0316	0.0003	0.0000
Autumn	0.0374	0.0005	0.0011	0.0423	0.0001	0.0000	-0.0058	0.0002	0.0000
$EC_{t,r}^{06}$	0.0843	0.0011	0.0041	6.5674	0.0018	0.0011	-1.6312	0.0019	-0.0001
Winter	0.0207	0.0003	0.0010	1.6912	0.0005	0.0003	-0.4335	0.0005	0.0000
Spring	0.0230	0.0003	0.0011	1.5261	0.0004	0.0002	-0.3766	0.0005	0.0000
Summer	0.0151	0.0002	0.0008	1.9419	0.0005	0.0003	-0.5146	0.0005	0.0000
Autumn	0.0255	0.0003	0.0012	1.4081	0.0004	0.0002	-0.3065	0.0005	0.0000
$EC_{t,r}^{12}$	0.0041	0.0001	0.0004	5.0955	0.0015	0.0020	-3.0245	0.0010	0.0000
Winter	0.0014	0.0000	0.0001	1.0798	0.0003	0.0005	-0.7097	0.0002	0.0000
Spring	0.0011	0.0000	0.0001	1.4383	0.0004	0.0005	-0.7510	0.0003	0.0000
Summer	0.0002	0.0000	0.0000	0.9086	0.0003	0.0004	-0.6421	0.0002	0.0000
Autumn	0.0013	0.0000	0.0001	1.6688	0.0005	0.0006	-0.9216	0.0003	0.0000

Note: The table presents the average contributions of climate features to predicted outcomes across all models utilising MIDAS-based feature extraction. For linear models, regression coefficients are reported, while for ML models, the average SHAP values are used to quantify feature importance. Climate-related features are shown with headline contributions (highlighted in grey), decomposed into own region, geographic compounding, and event compounding types (highlighted in blue), and further decomposed by seasonality, based on factor loadings derived from the estimated beta-polynomial weighting scheme.
Source: Authors' calculations.

Table A.17: GVA by Main NACE Sectors in the EU, 2002–2022

	Agriculture, Forestry and Fishing		Industry (Except Construction and Manufacturing)		Manufacturing		Other Sectors		Total
Year	Amount	(%)	Amount	(%)	Amount	(%)	Amount	(%)	Amount
2002	175,442.20	2.29	230,925.40	3.01	1,420,418.90	18.50	5,850,873.20	76.21	7,677,659.70
2003	174,078.30	2.21	235,603.90	2.99	1,422,988.60	18.05	6,051,339.00	76.75	7,884,009.80
2004	183,063.00	2.22	253,660.60	3.08	1,471,371.60	17.86	6,330,207.90	76.84	8,238,303.10
2005	167,801.80	1.96	270,051.90	3.15	1,509,373.60	17.59	6,631,850.60	77.30	8,579,077.90
2006	167,181.50	1.85	291,950.70	3.22	1,592,397.30	17.58	7,005,962.90	77.35	9,057,492.40
2007	182,870.30	1.90	300,733.10	3.13	1,696,625.80	17.64	7,438,761.20	77.33	9,618,990.40
2008	182,084.10	1.83	333,893.80	3.35	1,688,467.00	16.94	7,765,239.60	77.89	9,969,684.50
2009	158,700.30	1.66	321,667.50	3.36	1,465,198.00	15.32	7,619,840.10	79.66	9,565,405.90
2010	177,445.00	1.79	345,265.00	3.49	1,588,698.50	16.07	7,775,961.00	78.65	9,887,369.50
2011	192,257.20	1.89	346,391.00	3.40	1,677,402.60	16.46	7,976,189.20	78.26	10,192,240.00
2012	191,562.40	1.87	362,390.10	3.54	1,662,859.80	16.24	8,023,742.50	78.35	10,240,554.80
2013	196,504.60	1.90	352,150.80	3.40	1,663,827.60	16.09	8,130,955.20	78.61	10,343,438.20
2014	198,061.90	1.87	335,365.60	3.17	1,732,434.20	16.38	8,312,416.30	78.58	10,578,278.00
2015	197,466.30	1.80	327,305.40	2.98	1,870,018.90	17.04	8,576,958.40	78.17	10,971,749.00
2016	197,711.90	1.76	322,078.20	2.86	1,929,182.30	17.14	8,805,655.80	78.24	11,254,628.20
2017	219,056.70	1.87	331,478.60	2.83	2,001,123.70	17.07	9,172,950.90	78.24	11,724,609.90
2018	215,638.50	1.78	343,664.80	2.83	2,055,885.00	16.95	9,513,354.50	78.44	12,128,542.80
2019	221,308.10	1.76	361,946.80	2.88	2,100,840.90	16.71	9,891,070.90	78.66	12,575,166.70
2020	216,139.10	1.78	357,688.00	2.94	1,975,895.20	16.27	9,597,354.10	79.01	12,147,076.40
2021	232,784.10	1.77	392,584.10	2.98	2,177,299.70	16.53	10,372,045.10	78.73	13,174,713.00
2022	272,090.10	1.87	506,987.70	3.49	2,408,249.60	16.59	11,327,851.50	78.04	14,515,178.90
Average	196,154.64	1.89	329,703.95	3.15	1,767,169.47	16.90	8,198,599.04	78.06	10,491,627.10

Note: Annual data, current prices (million euro), GVA (ESA 2010), for the EU (27 countries, from 2020).
Source: Eurostat (2026).

Acknowledgements

As laureate of the 2023 hackathon on Climate Change, the authors express their special thanks to the organisers of the event: the ECB, Banque de France, Banca d'Italia, and the Copernicus services from the European Commission.
This paper should not be reported as representing the views of the authors' national banks, the ECB or the Eurosystem.

Sarah Spiteri
Central Bank of Malta, Valleta, Malta; email: spiterisr@centralbankmalta.org

Léonore Lebouteiller
Banque Centrale du Luxembourg, Luxembourg, Luxembourg; email: leonore.lebouteiller@bcl.lu

Nicole Vorderobermeier
Deutsche Bundesbank, Frankfurt am Main, Germany; email: nicole.vorderobermeier@bundesbank.de

Mar Delgado-Téllez
Banco de España, Madrid, Spain; email: mar.delgado@bde.es

Andrej Ceglar
European Central Bank, Frankfurt am Main, Germany; email: andrej.ceglar@ecb.europa.eu

Postal address 60640 Frankfurt am Main, Germany
Telephone +49 69 1344 0
Website www.ecb.europa.eu

PDF ISBN 978-92-899-7906-1 ISSN 1725-2806 doi:10.2866/5560446 QB-01-26-149-EN-N